

# Non-Metallic Material Science



## **Editor-in-Chief**

**Dr. Ali Durmus**

Istanbul University Cerrahpasa, Turkey

## **Editorial Board Members**

- |  |   |
|--|---|
| Ali Solati, Iran                         | Amid Ranjkesh, Korea                      |
| Lijian Meng, Portugal                    | Ning Luo, China                           |
| Edwin Peng, United States                | Kotari Srinivasarao, India                |
| Praveen Malik, India                     | Mostafa Ragab Abd El Wahab, Egypt         |
| Sofyan A. Taya, Palestinian              | N. Jeyaprakash, Taiwan                    |
| Hussein Mohammed Ali Ibraheem, Iraq      | Antonio Bastos Pereira, Portugal          |
| Samuel Paul David, Czech Republic        | G. Udhaya Sankar, India                   |
| Hongyu Liu, China                        | Alexander Pyatenko, Japan                 |
| Sayed Faheem Naqvi, India                | Andreas Rosenkranz, Germany               |
| Dan Dobrotă, Romania                     | Ashok Panchapakesan, India                |
| Manawwer Alam, Saudi Arabia              | Zhongchang Wang, Portugal                 |
| Nasrin Oroujzadeh, Iran                  | Lei Zhai, United States                   |
| Nikolai Stoyanov Boshkov, Bulgaria       | Laifa Shen, Germany                       |
| Alisa Buchman, Israel                    | Noel Ibrahim Akos, Nigeria                |
| Yuhuan Fei, China                        | Chih-Ta Tsai, Taiwan                      |
| Jasbeer Singh Satwant Singh Sidhu, India | Moonis Ali Khan, Saudi Arabia             |
| Chol-Hyon Kim, Korea                     | Hongyang Ma, China                        |
| Shivani Dhall, India                     | Upenyu Guyo, Zimbabwe                     |
| Mallinath Shrimanth Birajdar, India      | Soumya Mukherjee, India                   |
| Azam Sobhani, Iran                       | Muhammad Imran Rashid, Pakistan           |
| Yunyan Zhang, United Kingdom             | Cheng-Fu Yang, Taiwan                     |
| Prabakaran M P, India                    | Miaoxiang Chen, Sweden                    |
| Nastaran Parsafard, Iran                 | Ana Queirós Barbosa, Portugal             |
| Mohammad Sirousazar, Iran                | Sikiru Oluwarotimi Ismail, United Kingdom |
| Suha K. Shihab, Iraq                     | Mohammad Rashed Iqbal Faruque, Malaysia   |
| Kishore Debnath, India                   | Saeed Zeinali Heris, Iran                 |
| Hong-Liang Dai, China                    | Jelena Dragoslav Jovanovic, Serbia        |
| Tao Huang, United States                 | Jean-Paul Moshe Lellouche, Israel         |
| Shoujun Wu, China                        | Zilong Zhao, China                        |
| Amjad Khabaz, Turkey                     | Guoquan Nie, China                        |
| Linda Aissani, Algeria                   | Aline Teixeira de Souza, Brazil           |
| Seifollah Jamalpour, Iran                | Fellah Mammoun, Algeria                   |
| Emad Mohamed M. Ewais, Egypt             | Ahmad Ali Mousa, Jordan                   |
| Marco Vinicius Chaud, Brazil             | Nourredine AïT Hocine, France             |
| Samson Jerold Samuel Chelladurai, India  | Umberto Prisco, Italy                     |
| Nasser Sepehri Javan, Iran               | Hoejin Kim, University of Texas           |
| Prabhakaran Subramaniyan, France         | Srijita Bharti, India                     |
| Padmanabhan Krishnan, India              | Stefania Pasquale, Italy                  |
| Pradeep Lancy Menezes, United States     | Rouholah Ashiri, Iran                     |
| Sivakumar Dhar Malingam, Malaysia        | Ning Wu, China                            |
| Sina Matavos-Aramyan, Iran               | Shen Liu, China                           |
| Arafa Hussien Aly, Egypt                 | Morteza Ehsani, Iran                      |
| Mohammad Farooq Wani, India              | Anshu Sharma, India                       |
| Rishi Kumar, India                       | Chul Ho Park, Korea                       |
| Sourav Kundu, India                      | Hamid Reza Taghiyari, Iran                |
| Ravi Shanker Vidyarthi, India            | Latefa Sail, Algeria                      |

Volume 1 Issue 2 • October 2019 • ISSN 2661-3301 (Online)

# Non-Metallic Material Science

**Editor-in-Chief**  
Dr. Ali Durmus



**BILINGUAL  
PUBLISHING CO.**  
Pioneer of Global Academics Since 1984

## Contents

### Editorial

**1 A Foreword from the Editor-in-Chief**

Ali Durmus

### Article

**2 The Effect of Methacrylic Acid and Maleic Acid on the Isothermal Kinetics of Acrylic Acid Crosslinking Co-polymerization under Conventional and Microwave heating**

Jelena Jovanovic Borivoj Adnadjevic

**10 Thermo-Chromic Response of Polymer Stabilized Cholesteric Liquid Crystal for Thermal Imaging**

Rishi Kumar KK Raina

### Review

**15 Cellulose Acetate Reverse Osmosis Membranes for Desalination: A Short Review**

Shuo Liu Lifen Hu Wencai Zhang Hongyang Ma

**26 A Parametric Approach to the Evaluation of Flexural Strength of Advanced Ceramic or Glass Like Cylindrical Rods at Ambient Temperature**

Padmanabhan Krishnan

## Copyright

*Non-Metallic Material Science* is licensed under a Creative Commons-Non-Commercial 4.0 International Copyright (CC BY- NC4.0). Readers shall have the right to copy and distribute articles in this journal in any form in any medium, and may also modify, convert or create on the basis of articles. In sharing and using articles in this journal, the user must indicate the author and source, and mark the changes made in articles. Copyright © BILINGUAL PUBLISHING CO. All Rights Reserved.



## EDITORIAL

# A Foreword from the Editor-in-Chief

**Ali Durmus\***

Istanbul University Cerrahpasa, Turkey

---

### ARTICLE INFO

---

#### *Article history*

Received: 31 October 2019

Accepted: 1 November 2019

Published Online: 1 November 2019

---

I am very happy to announce that the *Non-Metallic Material Science (NMMS)* which is an open access and multidisciplinary academic journal and a technical platform bringing out original research work and covering all aspects of non-metallic materials, has started its publication journey by the Bilingual Publishing Co., in 2019. The scope of the journal is devoted to publish original experimental and theoretical research papers, reviews, short communications, and technical notes mainly in the areas of polymeric materials, composites and hybrid materials, inorganic and carbon-based materials.

The NMMS journal successfully published two issues in its year of birth, 2019. This second issue of first volume, Volume:1 (2), reported four articles in the areas of polymeric and ceramic materials, two are research papers and two are review papers. The paper by Jovanovic and Adnadjevic provided important kinetic data for the polymerization of acrylic copolymers. They have also discussed on the effect of microwave heating on the copolymerization reaction. The paper by Kumar reported thermo-chromic responses of polymer stabilized cholesteric liquid crystal and using of such system in thermal imaging applications. The paper by Liu et al. reviewed well the structural and physical properties of cellulose acetate reverse

osmosis membranes and their application performances in desalination processes. Krishnan suggested a parametric approach for evaluating of flexural strength of advanced ceramic or glass like cylindrical rods. We appreciate all the authors and reviewers who technically supported to the journal this year. We are very conscious of the point that the journal is still infant and needs invaluable supports of editorial board members. We are also aware of the case that we should work hard to expand the journal to a large scientific community in the relevant areas.

We have been working on making the submission and reviewing processes easier and faster compared to other open access journals. The NMMS journal is currently indexed by the important and popular scientific databases. We believe that the NMMS journal will be indexed by many scientific databases within a few years, in addition to the present databases.

I kindly invite you to submit your manuscripts to the upcoming issues of journal in 2020.

**Kind regards,**  
**Dr. Ali DURMUS**  
Editor-in-Chief

---

\*Corresponding Author:

Ali Durmus,

Istanbul University Cerrahpasa, Turkey;

Email: [durmus@istanbul.edu.tr](mailto:durmus@istanbul.edu.tr)

**ARTICLE**

# The Effect of Methacrylic Acid and Maleic Acid on the Isothermal Kinetics of Acrylic Acid Crosslinking Co-polymerization under Conventional and Microwave heating

**Jelena Jovanovic\*** **Borivoj Adnadjevic**

University of Belgrade, Faculty of Physical Chemistry, Studentski trg 12-16, 11000 Belgrade, Serbia

**ARTICLE INFO***Article history*

Received: 26 March 2019

Accepted: 12 August 2019

Published Online: 30 October 2019

*Keywords:*

acrylic acid (AA)

methacrylic acid (MA)

maleic acid (MAL)

isothermal crosslinking co-polymerizations

conventionally heating (CH)

microwave heating (MWH)

**ABSTRACT**

The kinetics of free-radical crosslinking co-polymerization (FRCCP) of acrylic acid (AA) with both methacrylic acid (MA) (PAMA hydrogel) and maleic acid (MAL) (PAMAL hydrogel) was investigated under the conditions of isothermal conventional heating (CH) and under the conditions of microwave heating (MWH) with controlled cooling. The kinetics curves of FRCCP of PAMA and PAMAL hydrogels under the conditions of CH are described with the kinetics model of second order chemical reaction, whereas the kinetics curves under the conditions of CH are described with the kinetics model of Polany-Winger. It is proved that MWH leads to the changes in the rate of FRCCP and to the changes in the values of the kinetic parameters (activation energy ( $E_a$ ) and pre-exponential factor ( $\ln A$ )). It was found the existence of relationship between the values of the kinetic parameters calculated for MWH and CH for PAMA and PAMAL hydrogel synthesis process, which is well-known as compensation effect. The effect of MWH on the kinetics of FRCCP for PAMA and PAMAL hydrogel formation were explained by applying the model of activation by selective energy transfer (SET). The changes in kinetics model, rate of FRCCP and kinetics parameters, caused with the MWH can found wide application in designing novel technologies for obtaining polymers and for synthesis of polymers with novel physico-chemical properties. The suggested mechanism of activation for polymerisation under the conditions of MWH also enables development of novel reaction systems and technologies for polymers productions.

**1. Introduction**

Hydrogels present a novel class of non-metallic materials which attract significant attention during last two decade. Hydrogels are usually defined as 3-D networks of hydrophilic polymers which absorb huge amounts of water, water solutions and biological liquids without to dissolve neither to

lose physical or chemical stability. Thanks to their distinguishing properties (hydrophilicity, biocompatibility, high swelling degree in water and water solutions, low or complete nontoxicity) and to capabilities to respond to different changes in medium by which are surrounded, hydrogels found widespread applications in different fields such as: bio-medical, pharmaceutical,

*\*Corresponding Author:*

Jelena Jovanovic,

University of Belgrade, Faculty of Physical Chemistry, Studentski trg 12-16, 11000 Belgrade, Serbia;

Email: [jelenaj@ffh.bg.ac.rs](mailto:jelenaj@ffh.bg.ac.rs)

agrochemical and environmental <sup>[1]</sup>. The most important method for hydrogel synthesis is free-radical crosslinking polymerizations (FRCP) under the conventional heating (CH) where the kinetics of hydrogel formation is followed isothermally <sup>[2]</sup>.

Microwave heating (MWH) is nowadays well-known non-conventional source of energy which is applied in various field of chemistry, especially organic <sup>[3]</sup> and polymer synthesis <sup>[4]</sup>, material science <sup>[5]</sup> and various physicochemical processes <sup>[6,7,8]</sup>. The advantages of using MWH in synthetic purposes are connected with the facts that: MWH considerably accelerates the reactions rate, enhances the yields of desired product giving products with better properties. Accordingly, application of microwaves appeals more attention <sup>[9]</sup>. The influence of microwaves on the kinetics of chemical reactions was predominantly explained by thermal effects (overheating, hot-spots, selective heating) as well as by specific microwave effects <sup>[9,10]</sup>.

Among the earliest application of microwave heating was reported in 1968 <sup>[11]</sup> as unconventional method for poly(methyl methacrylate) (PMMA) processing as alternative to common processing using water-bath heating <sup>[12]</sup>. The initially used MWH to polymerize methyl methacrylate (MMA) exhibited substantial decrease in polymerization time from 9 hours to just 3 minutes, at the same time giving same properties of synthesized PMMA as in the case of CH <sup>[11,13,14]</sup>. A comprehensive review was nicely presented the actual literature overview and the perceptions of MWH in synthesis of polymers <sup>[15]</sup>. The atom transfer radical polymerizations (ATRP) of MMA under controlled MWH was performed and gave vary similar results to the ones obtained under CH which was a good indication that there is not "microwave effect" in the MWH ATRP. The considerable reactions rate acceleration over CH was explained <sup>[16]</sup>. A comparative analyses of the CH and MWH kinetics of MMA polymerization was performed, which reveals that the polymerization rates increased under the MWH up to 8.9 times. The kinetics parameters for MMA polymerization for the MWH conditions were 1.2-12 times lower than comparable for CH conditions and they were dependent on the degree of polymerization. The decreased value of activation energy ( $E_a$ ) of MWH polymerization is explained with the non-equilibrium energetic distribution of the reactants <sup>[17]</sup>. Spasojevic and co-workers investigated the effects of isothermal heating modes, CH and MWH, on the kinetics of polymerization and the properties that are significant for the application of several PMMA base dental materials commercially available. It was found that the use of MWH in provokes the changes in the kinetics model of

polymerization, the values of rates constants which are ~4 times higher than in the case of CH polymerization and the values of kinetics parameters (activation energy and pre-exponential factor) which are lower for the MWH polymerization <sup>[18,19]</sup>.

In the literature are available reports about the preparation of superabsorbing materials under MWH from sodium acrylate, corn starch, and poly(ethylene glycol) diacrylate <sup>[20]</sup>. Superabsorbents were prepared by using sodium acrylate, starch, and 2-acrylamido-2-methylpropanosulfonic acid. Then, the copolymerization was more rapidly under MWH and the obtained products exhibited higher swelling rates than in the case of CH synthesized products <sup>[21]</sup>. The microwave-assisted preparation of poly(N-iso-propylacrylamide) (PNIPAAm) hydrogel with improved responsive properties was described. It was found that the MWH hydrogel synthesis under 75 W was finished in only 40 sec giving 99 % yield <sup>[22]</sup>. Z. Zhao and co-workers showed that the use of MWH considerably enhanced the reaction rate for PNIPAAm hydrogel synthesis from the hours to a few minutes and achieved the yields up to 99%. Additionally, the obtained PNIPAAm hydrogels synthesized under MWH had more porous structure and had higher swelling degree <sup>[23]</sup>.

The grafting of acrylic acid (AA) onto chitosan under MWH was investigated. It was shown that the MWH leads to the increase in the reaction rate up to the 8 times in comparison to the CH method giving the grafting degree and grafting efficiency of the obtained product similarly to the grafting in CH method <sup>[24]</sup>. MWH has been successfully used to obtain chitosan-g-poly (acrylonitrile) without use of initiator during the only 1.5 min <sup>[25]</sup>. Graft copolymer of  $\kappa$ -caragenan with methyl methacrylate was synthesized with high yield by using potassium-persulfate as an initiator. It was confirmed that controlled MWH can be used for the preparation of stable copolymer of  $\kappa$ -caragenan <sup>[26]</sup>.

In the work of Jovanovic and Adnadjevic, the isothermal kinetics of the overall crosslinking polymerization of acrylic acid (CPAA) in a CH and MWH reaction process of poly (acrylic acid) (PAA) hydrogel preparation was examined. In the MWH polymerization the reaction rate constant of PAA hydrogel formation increases 32- 43 times, when compared to the CH process. The kinetics of the isothermal PAA hydrogel formation during the MWH process was successfully described by the kinetics model of first-order chemical reaction, on the contrary to CH process when the isothermal kinetics is completely described with the second-order chemical reaction rate model. Furthermore, the reaction kinetics of the PAA hydrogel formation in the MWH is changed as well as its kinetic

parameters. The activation energy ( $E_a$ ) was decreased ~19% and the pre-exponential factor ( $\ln A$ ) ~2.2 times<sup>[27]</sup>. Adnadjevic et. al established that the increase in the reaction rate of CPAA for MWH was not caused with the overheating neither with the existence of hot spots in the investigated reaction system. The offered explanation of the effects of MWH on the kinetics of CPAA is based on the specific mode of activation of model of reacting molecules<sup>[28]</sup>. Nikolic and co-workers presented new synthesis of poly(D,L-lactide) under controlled MWH<sup>[29]</sup>.

In spite of the huge practical significance of the hydrogels as smart materials, the investigations of the kinetics of hydrogel preparation by simultaneous crosslinking polymerization under the isothermal MWH are sparse. There are no works about the synthesis of AA copolymer hydrogels nor the kinetics of FRCCP of the AA acid with MA and AA acid with MAL, under CH and MWH. Therefore, this work investigates for the first time in the literature the effects of methacrylic acid (MA) and maleic acid (MAL) as copolymer units, on the kinetics of the AA copolymerization under CH and MWH.

In regard with that, the aim of this investigation was to determine the kinetics model, kinetics parameters and kinetics complexity and based on them offer the elucidation of the effect of MWH. This paper offers the knowledge about the kinetics of FRCCP under the CH and under the influence of MWH which is important for understanding the kinetics of polymerisation reaction under the MWH and for the advancement of the polymerisation technologies. Furthermore, the knowledge of the kinetics is of crucial importance for the design and projecting scale-up plant.

## 2. Experimental

### 2.1 Materials

The monomers, acrylic acid (AA) (99 wt %), methacrylic acid (MA) (99 wt%) and maleic acid (MAL) were purchased from Merck, Germany. The crosslinker, N,N-methylene bisacrylamide (p.a) (MBA) was obtained from Aldrich Chemical, USA. The 2,2-azobis-[2-(2-imidazolin-2-il)-propane] dihydrochloride, which was used as an initiator, was supplied by Wako Pure Chem. Ind., Japan. Double distilled water was used through the all synthesis.

### 2.2 Hydrogel Synthesis

Both poly(acrylic acid-co-methacrylic acid) hydrogel (PAMA) and poly(acrylic acid-co-methacrylic acid) (PAMAL) hydrogel were synthesized by the free-rad-

ical crosslinking co-polymerization of AA, actually using the same procedures. The synthesis of PAMA hydrogel was described in details in our previous papers<sup>[30]</sup>. The prepared reaction mixture was putted into glass test tubes which were properly sealed and placed in a laboratory oven for predetermined time intervals. After the predetermined time interval, the reaction was stopped by placing test tube with reaction mixture in ice water. Subsequently, the resulting product – formed hydrogel was removed from the test tubes, sliced and immersed in tenfold volume excess of distilled water, in order to remove any sol-fraction. The water is changed each 3 hours, except overnight, during 7 days. Then, the washed-out samples of hydrogels were dried until unchanging weight, by the previously established procedure<sup>[30]</sup>. Actually, the washed-out hydrogel was dried in an air oven in a temperature regime of 353 K for 2 h, 363 K for 3 h, and 378 K until the sample reaches a constant weight, according to our long-lasting experience the obtained best results. The obtained product (xerogel) was completely dry, opal white solid, and was stored in a desiccator until further use.

Hydrogels synthesis under MWH were performed in a modified microwave unit (Discover, CEM Corp., USA), whose construction and principle of work is described in details in the work of Adnadjevic et al<sup>[31]</sup>.

### 2.3 Determination of the Yield

The yield ( $Y$ , %) of the obtained hydrogel was determined by gravimetric method and calculated as:

$$Y = \frac{W_t}{W_0} \quad (1)$$

where the  $W_t$  is the mass of dried washed out hydrogel (xerogel) and the  $W_0$  is the mass of the used co-monomers.

### 2.4 Model-Fitting Method

The kinetics and kinetics models of the investigated reactions were determined by model-fitting method<sup>[32]</sup>. Detailed description of kinetics models determination based on using experimentally conversion curves is given in our previous works<sup>[30,31]</sup>.

## 3. Results and Discussion

The conversion curves of PAMA hydrogel (the dependence of the yield on polymerization time) obtained under isothermal conventionally heated conditions at different temperatures are shown in Figure 1.

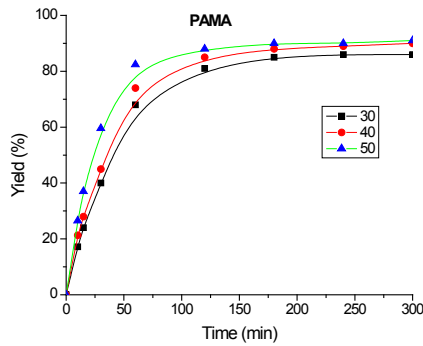


**Figure 1.** Conversion curves of PAMA hydrogel at CH conditions

The shape of conversion curves of PAMA hydrogel is complex and independent on temperature of polymerization. For all the conversion curves at short reaction times the yield of the obtained hydrogel product rapidly and linearly increases with time, followed with convexly decrease, until attaining the plateau at long times. The maximal achieved yield of the PAMA hydrogel was ~ 90%. The increasing temperature leads to the increase in both the slope of the linear part of conversion curve and the time to reach plateau decrease. The increase in the value of the slope of linear part of conversion curves and decrease in time required to reach the plateau indicates that the polymerization process is thermally activated one whose rate increase with the increasing temperature.

By using the “model-fitting” method it was concluded that the kinetics curves can be described with the kinetics model of second order chemical reaction, given with Equation (2):

$$Y = \frac{kt}{1 + kt} \tag{2}$$

where the  $k$  is the rate constant. In order to calculate the  $k$ , the Eq (2) is linearized in the form of dependence of the  $t/Y$  on time.

The dependence of  $t/Y$  on time of PAMA hydrogel at different temperatures at CH conditions is shown in Figure 2.

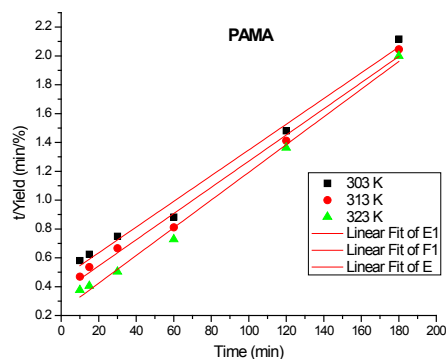


**Figure 2.** The dependence of  $t/Y$  on time for PAMA hydrogel

The dependence of  $t/Y$  on time for all of the temperatures provides straight lines for the whole range of the reaction. Since the dependence is straightforward within the entire range, from their slopes are calculated the values of rate constant  $k$  for each temperature. Table 1 presents the isothermal values of  $k$  for PAMA hydrogel at CH conditions at different temperatures.

**Table 1.** The values of  $k$  for PAMA and PAMAL hydrogel at CH conditions

	PAMA	PAMAL
T, K	$k, \text{min}^{-1}$	$k, \text{min}^{-1}$
303	2.19	0.68
313	2.76	0.98
323	4.32	1.28

From the results given in Table 1 it is obvious that the values of  $k$  for PAMA hydrogel formation increase with the increasing reaction temperature. Since the changes in the values of  $k$  are in agreement with the Arrhenius Equation, the values of kinetics parameters, activation energy ( $E_a$ ) and pre-exponential factor ( $\ln A$ ) are calculated by applying it. The calculated values of kinetics parameters are found to be:  $E_a=27.5 \text{ kJ/mol}$  and  $\ln(A/\text{min}^{-1})=11.7$ .

Figure 3 shows the isothermal conversion curves of PAMA hydrogel formation under MWH conditions at different temperatures.

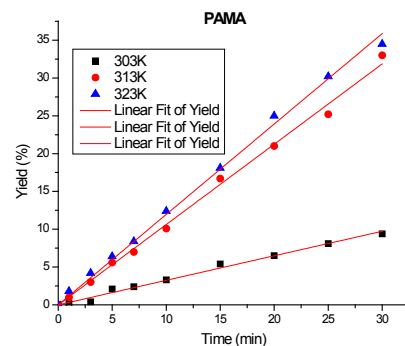


**Figure 3.** The conversion curves of PAMA at MWH conditions

The conversion curves of PAMA at MWH conditions have different shape than the conversion curves obtained under the CH conditions. The yield of PAMA linearly increase with the increase in duration of polymerization for all the temperatures. The application of the “model-fitting” method indicates that the kinetics curves of PAMA polymerization at MWH conditions should be described by using Polany –Winger mode, given with Equation (3):

$$Y = kt \tag{3}$$

Table 2 presents the isothermal values of  $k$  for PAMA and PAMAL hydrogel at MWH conditions at different

temperatures.

**Table 2.** The values of  $k$  for PAMA and PAMAL hydrogel at MWH conditions

T, K	PAMA $k, \text{min}^{-1}$	PAMAL $k, \text{min}^{-1}$
303	0.342	2.242
313	1.035	3.058
323	1.246	3.756

The results given in Table 2 reveals that the values of the  $k$  for PAMA hydrogel at MWH conditions increasing with the reaction temperature in compliance with Arrhenius equation, as in previous case of CH conditions. The kinetics parameters values, activation energy and pre-exponential factor, for PAMA at MWH conditions were calculated as following:  $E_a=50.1 \text{ kJ/mol}$  and  $\ln(A/\text{min}^{-1}) = 20.9$ .

By comparing kinetics data for PAMA hydrogel at CH and MWH conditions one can conclude the following. The MWH most probably provokes the alteration in the kinetics model of FRCCP of AA and MA, the decrease in the value of the  $k$  and leads to the increase in the values of kinetics parameters. A functional relationship between the kinetics parameters for at CH and MWH conditions is found and is expressed with following Equation:

$$\ln A = 0.471 + 0.408E_a \quad (4)$$

where  $E_{a,F}$  and  $\ln A_F$  are the activation energy and pre-exponential factor in a defined physical field [33]. By its form, Equation (4) is well-known as the Equation of the compensation effect, which is related to variations in the reactions settings.

By comparing kinetics data obtained for PAMA hydrogel with the results obtained for PAA hydrogel [28] it is clear that the introduce of methacrylic acid (MA) as co-monomer does not change the kinetics model, but provokes the decrease in the rate of polymerization and the increase in kinetic parameters, both under CH and MWH conditions.

The isothermal conversion curves of PAMAL hydrogel obtained under CH conditions at different temperatures are given in Figure 4.

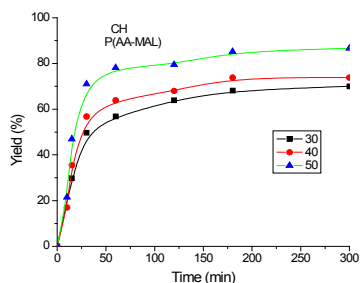


**Figure 4.** Conversion curves of PAMAL hydrogel at CH conditions

The conversion curves of PAMAL hydrogel have comparable forms for all experimental temperatures, showing the 3 distinct stages of the changes of the yield of the PAMAL hydrogel formation with time: a linear, non-linear (convexly) and plateau. As in the case of PAMA hydrogel, with the increase in temperature of polymerization the maximal yield of PAMAL hydrogel increase. At the start of the process, i.e. at short reaction times, the yield of the PAMAL hydrogel linearly and abruptly increases with time, after which slowed down, until reaching saturation at long limes. The slope of the linear part of the conversion curves increase with the increase in temperature, whereas the time to reach plateau decreases. As in the case of the PAMA hydrogel formation, these facts indicate that investigated FRCCP is thermally activated process.

The application of the “model-fitting” method reveals that the kinetics curves can be described by using the Equation (2), as in the case of PAMA. In accordance with that, the dependence of  $t/Y$  on time for PAMAL at CH conditions at different temperatures is investigated and presented in Figure 5.

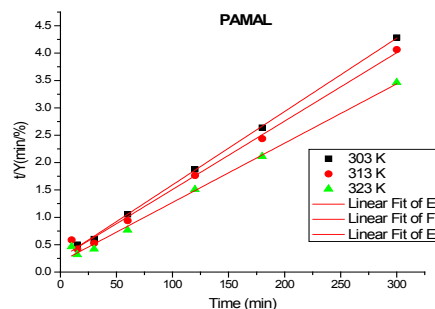


**Figure 5.** The dependence of  $t/Y$  on time for PAMAL

As obvious from Figure 5, the above dependency is straight within the whole range at all the temperatures. The values of the  $k$  are calculated based on the slopes of these dependencies. The calculated isothermal values of  $k$  for PAMAL formation at different temperatures at CH conditions are given in Table 1 (column 3). The increasing values of  $k$  with temperature are in agreement with the Arrhenius Equation, which allows calculation of the values of kinetics parameters, activation energy ( $E_a$ ) and pre-exponential factor ( $\ln A$ ). The calculated values of the kinetics parameters are:  $E_a=24.9 \text{ kJ/mol}$  and  $\ln(A/\text{min}^{-1})=9.5$ .

Figure 6 shows the isothermal conversion curves of PAMAL hydrogel obtained under MWH conditions at different temperatures.

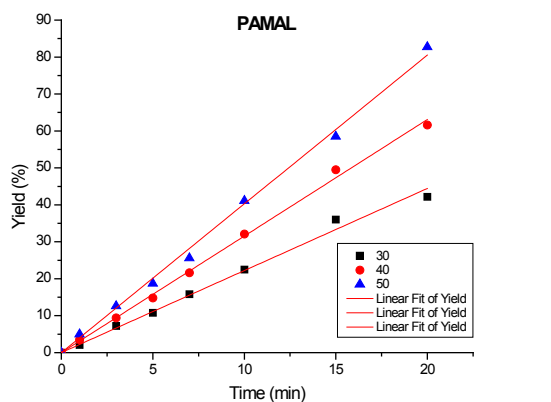


**Figure 6.** Conversion curves of PAMAL at MWH conditions

Similarly to the previously presented results for the PAMA at MWH conditions, the conversion curves are obviously linear, within the whole investigated range of PAMAL polymerization reaction. The dependence of the yield on reaction time for PAMAL at MWH can be described with the Equation (3).

The slope of the conversion curves, again, increase with the increase in reaction temperature, and from their values the values of  $k$  for PAMAL at MWH conditions at different temperatures are calculated (see Table 2). As in the previously explained cases, the values of kinetics parameters,  $E_a$  and  $\ln A$  at MWH conditions are calculated and found to be:  $E_a = 21.3 \text{ kJ/mol}$  and  $\ln(A/\text{min}^{-1}) = 9.2$ .

As in the case of the use of MA as co-monomer, the kinetics model of PAMAL polymerization under the MWH conditions is found to be different than under the CH conditions. On the contrary to the MA, in the case of PAMAL the MWH leads to the increasing rate constants values and to the decreasing kinetics parameters values in comparison to their values obtained under the CH conditions. Between the kinetics parameters of PAMAL at CH and MWH conditions it is found the existence of correlation relationship - compensation effect, given with following equation:

$$\ln A = 6.911 + 0.106E_a \quad (5)$$

The results presented in this manuscript enable to make comparison between the two types of co-monomers and their effects in the kinetics of the FRCCP under both CH and MWH conditions. On the other side, it is possible to discuss the effects of heating mode, CH or MWH on the kinetics of the investigated isothermal process. Under the CH conditions, it is possible to successfully describe the kinetics of both PAMA and PAMAL hydrogel formation

using same kinetics model, i.e. by the kinetics model of second order chemical reaction. The values of kinetics parameters are higher for PAMA. Under the MWH conditions, the kinetics of both PAMA and PAMAL hydrogel formation again can be successfully described by using the same kinetics model but different than in the case of the same processes under CH conditions, i.e. by Polanyi-Winger model. The values of kinetics parameters are higher for PAMA.

In the works of Adnadjevic, Jovanovic, et al, the so called “model of selective energy transfer (SET)” of activation of reactive molecules is presented, with aim to explain the effects of MWH on the kinetics of physico-chemical processes such as polymerization and dehydration [9,19,27,28,30,31]. In agreement with that model, in the case when exists compensation effect between the calculated values of kinetics parameters obtained under different modes of heating of reaction system, it is possible to calculate the values of: the anharmonicity constant ( $x$ ), resonant vibration mod of monomers molecule ( $\nu$ ) and the vibration quantum number ( $n$ ). The calculated values of  $\nu$ ,  $n$  and  $x$  for PAMA and PAMAL hydrogel formation under MWH and CH are given in Table 3.

**Table 3.** The values of  $\nu$ ,  $n$ , and  $x$  for PAMA and PAMAL hydrogel formation

Variable	PAMA		PAMAL	
	CH	MW	CH	MW
$\nu/\text{cm}^{-1}$	410	410	1579	1579
$n$	6	10	2	1
$x$	-0.025	$-3.45 \times 10^{-3}$	-0.204	$-7.9 \times 10^{-3}$

From the results given in Table 3, it is indicating that in the case of PAMA hydrogel formation, both under CH and MWH, the resonant transfer of energy takes places at vibration mode with wave number  $\nu = 410 \text{ cm}^{-1}$ , which matches to the skeletal vibrations of the monomer unit -C-C-C- of AA and MA. In contrast to this, in the case of PAMAL resonant transfer of energy takes places at vibration mode with wave number  $\nu = 1579 \text{ cm}^{-1}$ , which corresponds to stretching asymmetric vibrations of carboxylic group C-O-O of the monomer unit of AA and MAL.

The increase in the value of  $E_a$  and  $\ln A$  under MWH in comparison with the CH in the case of PAMA hydrogel is related with the quant nature of activation energy and can be explained with the higher number of the necessary quant of energy and with the higher value of the anharmonicity factor. That increase happened due to the specific interaction of MW irradiation with the molecules of methacrylic acid. The decrease in the value of  $E_a$  and  $\ln A$  under MWH in the case of PAMAL hydrogel is also relat-

ed with the quant nature of activation energy and can be explained with the lower number of the necessary quant of energy and with the lower value of the anharmonicity factor. That decrease happened due to the specific interaction of MW irradiation with the molecules of maleic acid.

#### 4. Conclusions

(1) The kinetics of FRCCP of PAMA and PAMAL hydrogel under the CH conditions is described with the kinetics model of second order chemical reaction.

(2) The kinetics of FRCCP of PAMA and PAMAL hydrogel under the MWH conditions is described with the kinetics model of Polany-Winger.

(3) The type of co-monomer does not affect the kinetics model within the same heating mode.

(4) The MWH provokes the alteration in the kinetics model of crosslinking co-polymerization for both comonomers in comparison to the CH.

(5) The type of commoner effects on the values of kinetics parameters for both CH and MWH.

(6) The values of  $E_a$  and  $\ln A$  are under the conditions of MWH in comparison to the CH are higher for PAMA and lower for PAMAL.

(7) The relationships among the kinetic parameters values for MWH and CH conditions for both FRCCP are present (compensation effect).

(8) The resonant transfer of energy during crosslinking co-polymerization for PAMA formation takes places at vibration mod with wave number  $\nu = 410 \text{ cm}^{-1}$ , both under CH and MWH, which corresponds to the skeletal vibrations of the monomer unit -C-C-C- of AA and MA. In contrast to this, in the case of PAMAL hydrogel, resonant transfer of energy takes places at wave number  $\nu = 1579 \text{ cm}^{-1}$ , which corresponds to stretching asymmetric vibrations of carboxylic group C-O-O of the monomer unit of AA and MAL.

(9) The activation energy for both co-monomers is quantized value and it is determined with the number of quanta exchanged throughout the selective transfer of energy.

(10) The application of MWH opens wide perspectives for designing novel, cost effective technologies for products based on polymers.

(11) The application of SET model mechanism of activation leads to the development of novel polymerization reaction systems.

#### Acknowledgement

This investigation was supported by the Ministry of Science and Technical Development of the Republic of

Serbia, through Project No. 172015 OI.

#### References

- [1] N.A. Peppas, B.V. Slaughter, M.A. Kanelberger, *Polymer Science: A comprehensive reference, Hydrogels*. Polym. Biol.Med., 2012, 9: 385–395.
- [2] B. Adnadević, J. Jovanović: *Hydrogels – Synthesis, Structures and Properties*, Monography and additional scholar book, Faculty of Physical Chemistry, Belgrade, 2014: 253. ISBN: 978-86-82139-46-1
- [3] C.O. Kappe, D. Dallinger, and S.S. Murphree, *Practical Microwave Synthesis for Organic Chemists—Strategies, Instruments, and Protocols*, Wiley-VCH, Weinheim, 2009.
- [4] D. Bogdal and A. Prociak, *Microwave-Enhanced of Polymer Chemistry and Technology*, Blackwell, Oxford, UK, 2007.
- [5] S. Singh, D. Gupta, V. Jain, and A.K. Sharma, *Mater. Manuf. Process.*, 2015, 30, 1.
- [6] A. Saberi, F. Golestani-Fard, M. Willert-Porada, Z. Negahdari, C. Liebscher, and B. Gossler, *Ceramics Internat.*, 2009, 35(933).
- [7] H.J. Sung, J. Taihuan, K. Young, and C. Jong-San, *Chem. Eur. J.*, 2007, 13(4410).
- [8] Q.S. Liu, T. Zhang, N. Li, P. Wang, and G. Abulkemi, *Appl. Surface Sci.*, 2010, 256(3309).
- [9] B. Adnadjevic and J. Jovanovic, *The Effect of Microwave Heating on the Isothermal Kinetics of Chemicals Reaction and Physicpchemical Processes*, in *Advances in Induction and Microwave Heating of Mineral and Organic Materials*, Prof. G. Stanislaw, Ed., InTech Europe, Rijeka, Croatia, Open Access Publisher, 2011.
- [10] A. de la Hoz, A. Diaz-Ortiz, and A. Moreno, *Chem. Soc. Rev.*, 2005, 34(164).
- [11] M. Nishii, *The Journal of Osaka University Dental School*, 1968, 2, 23-40.
- [12] R. L. Schneider, E.R. Curtis, J.M.S.Clancy, *J. Prosthetics Dentistry*, 2002, 88: 145-150.
- [13] N. Yunus, A. A. Rashid, L. L. Azmi, M. I. Abu-Hasan, *J.Oral Rehabilitation*, 2005, 32: 65-71.
- [14] C. M.Rizzaati-Barbosa, M. C. Robeiro da Silva, *J. Prosthodontics*, 2009, 18: 503-506.
- [15] F. Wiesbrock, R. Hoogenboom, U. S. Schubert, *Macromol. Rapid Commun.* 2004, 25: 1739–1764.
- [16] H. Zhang, U. S. Schubert, *Macromol. Rapid Commun.* 2004, 25: 1225–1230.
- [17] J. Jovanovic, B. Adnadjevic, *J. App. Pol. Sci.* 2007, 104: 1775-1782.
- [18] P. Spasojevic, B.Adnadjevic, S.Velickovic, J.Jova-

- novic, J. App. Pol. Sci. 2011, 119: 3598-3606.
- [19] P. Spasojevic, J. Jovanovic, B. Adnadjevic, Mat. Chem. Phys., 2013, 141 (2-3): 882-890.
- [20] T.Zheng, P.Wang, Z. Zhang, B. Zhao, J. Appl. Polym. Sci, 2005, 95: 264.
- [21] Xu, K.; Zhang, W. D.; Yue, Y. M.; Wang, P. X. J. Appl. Polym. Sc.i, 2005, 98: 1050,
- [22] Shi, S.-H.; Liu, L. J. Chin Chem Lett, 2006, 17(361).
- [23] Z. Zhao, Z. Li, Q. Xia, H. Xi, Y.Lin, Eur. Polym. J. 2008, 44(1217).
- [24] G.Hucui, P.Wan, L. Dengke, Carbohydr Polym, 2006, 66(372),
- [25] S.Vandana, N. T. Devendra,; T.Ashutosh, S. Rashmi, J. Appl. Polym Sci. 2005, 95(820).
- [26] K.Prasad, R. Meena, A. K. Sidhanta, J. Appl. Polym. Sci. 2006, 101(161).
- [27] J. Jovanovic, B. Adnadjevic, J. Appl. Polym. Sci. 2010, 116(55–63).
- [28] B. Adnadjevic, J. Jovanovic, and B. Potkonjak, Rus. J. of Phys. Chem. A, 2013, 87(13).
- [29] Lj. Nikolic, I. Ristic, B. Adnadjevic, V. Nikolic, J. Jovanovic, M. Stankovic, Sensors, 2010, 10: 5063-5073.
- [30] J. Jovanovic, B. Potkonjak, T. Adnadjevic, B. Adnadjevic, Polymer Engineering and Science, 2016, 56(1): 87-96.
- [31] B Adnadjevic, M Gigov, J Jovanovic, Chemical Engineering Research & Design, 2017, 122: 113-120.
- [32] M. E. Brown, D. Dollimore, A. K. Galway, Reaction in the Solid State, In Comprehensive Chemical Kinetics, Ed. Elsevier, 1980.

**ARTICLE**

# Thermo-Chromic Response of Polymer Stabilized Cholesteric Liquid Crystal for Thermal Imaging

**Rishi Kumar<sup>1,2\*</sup> KK Raina<sup>2</sup>**

1. Department of Physics, Guru Nanak College, Budhlada, 151502, India

2. School of Physics and Materials Science, Thapar University, Patiala, 147004, India

**ARTICLE INFO***Article history*

Received: 26 March 2019

Accepted: 12 August 2019

Published Online: 30 October 2019

*Keywords:*

Polymer stabilized cholesteric texture (PSCT)

Cholesteric liquid crystal (CLC)

Morphological study

Thermo-chromic Responses

**ABSTRACT**

Cholesteric liquid crystal (Ch-LC) exhibits many remarkable optical properties due to formation of a macroscopic helical structure. A low amount of monomer (5wt.%) is dispersed into cholesteric liquid crystal and get polymerized under UV radiations to form polymer stabilized cholesteric texture (PSCT). The thermo-chromic response made this device suitable for the developing applications in thermal imaging. Temperature based measurements of PSCT exploits the key property of some polymer stabilized cholesteric liquid crystals (PSCLC) to reflect definite colors at specific temperatures. The selective color of PSCT texture shifts with raise in temperature from 30oC to 85oC, which can be utilized in thermal imaging applications.

**1. Introduction**

Chirality is the necessary parameter to be thought of in polymer stabilised cholesteric liquid crystals for the display applications in technology like privacy windows, electrically controlled shutter, bistable reflective displays, color filters, Fresnel lens and thermally activated color imaging sensors [1-8]. Normally thermotropic liquid crystals consist of rod-like molecules show one or several additional mesophases in the temperature range between the crystalline, and the isotropic liquid state which is used for the development of liquid crystal based devices [9-12]. These mesophases are mostly category of fluids and their physical properties depend on the orientations of the molecules with characteristic phase. The smectic phases itself thought

of as chiral phases. However chirality in nematic phases is evoked by acceptable dispersions of chiral molecules in nematic liquid crystals [13-19], that forms layer structures. The French physicist, G. Friedel [8], delineated the cholesteric phase by introducing small amount of chiral non-ceramic compound into nematic phase. The key property for the configuration assignment of chiral molecules is that the induction of oppositely-handed cholesteric by enantiomers. Thermochromic liquid crystal devices exploit in show technologies on the idea of optical property of these chiral nematic phase. For the electro-optic application of liquid crystals in displays, Researchers [20-25] focused on the development of larger numbers of light modulated devices by doping of chiral molecules in polymer liquid crystal dispersions to

\*Corresponding Author:

Rishi Kumar;

Department of Physics, Guru Nanak College, Budhlada, 151502, India; School of Physics and Materials Science, Thapar University, Patiala, 147004, India;

Email: rishikumar.phd@gmail.com

form complex and stable polymer stabilized cholesteric textures (PSCT).

Polymer stabilized cholesteric liquid crystals (PS-LCs) can be created by dispersion of a small amount of photo-reactive monomers into a liquid crystal (LC) with low molar mass. Anisotropic polymer network is formed after ultraviolet (UV) light exposure. In most cases, the polymer network keeps the order of the LC environment from which it was formed originally and thence contributes to the electro-optic characteristics by providing alignment to the liquid crystal molecules. The various parameters like nature of liquid crystal and polymer, refractive index, liquid crystal anisotropy, curing temperature and intensity affects the electro optic performance of shutter devices. Most of the analysis work is currently dominant for controlling the color contrast and switching responses of these shutters which are formed by using acrylate polymers<sup>[26-30]</sup>.

In this paper, we have made an attempt to construct temperature sensing device by inducing chirality in polymer stabilized liquid crystal composite films. We investigated here thermo-chromic responses and characteristic states of PSCT textures with the assistance of optical microscopy, which can be helpful for the development of PSCLC composite film in thermal imaging.

## 2. Experiment

In this investigation, an active chiral dopant CB15 (M/S E. Merck Dramstadt, Germany) was doped (5 wt. %) into room temperature nematic liquid crystal BL036 (purchased from E. Merck, UK) for inducing chirality in the sample. Nematic LC (BL036) exhibits nematic-isotropic transition ( $T_{NI}$ ) at 95°C and show their characteristic optical properties such as birefringence ( $\Delta n$ ) 0.267 and extra ordinary refractive index ( $n_e$ ) 1.527. An optical adhesive NOA65<sup>[22]</sup> was mixed in very small amount (5 wt. %) for controlling the anisotropic network morphology in polymer stabilized cholesteric texture (PSCT). Refractive index of the dispersed NOA65 optical adhesive ( $n_p$ ) was 1.52. Now the composite mixture was sandwiched into two antiparallel planer aligned polyamide coated ITO glass substrate via capillary action on hot stage to form homogeneous composite film. Rubbing of polyamide film by nylon cloth encouraged the homogenous aligned liquid crystal molecules in antiparallel direction. Film thickness was controlled 5 $\mu$ m by using glass bead spacers. Then cell was sealed with optical adhesive epoxy glue. After that phase separation is achieved by curing the cell into UV radiations ( $I \sim 2\text{mW}/\text{cm}^2$ ) for an hour by polymerization induced phase separation (PIPS) technique<sup>[28-30]</sup>. Then sample cell was allowed to cool down

at room temperature. Electrical contact with conducting ITO substrate was created by using indium solder.

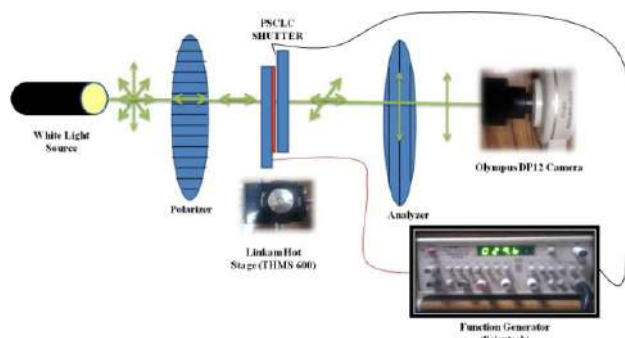


**Figure 1.** Experimental Setup for thermal analysis connected with optical microscope

Temperature dependence study of the sample cell was carried by heating the sample from room temperature @ 0.1°C/min with the help of Linkam controlled hot stage (Model TP94 and THMS600). Film morphology of PSCLC sample cell was studied under cross polarizer at 100X magnification through Olympus polarizing microscope (Model BX-51P) fitted with charge coupled device (CCD) camera interfaced with computer. Photomultiplier tube (Model RCA931-A) was used for measuring thermo-optic response of PSCLC sample under application of electric field by using function generator (Model Scientech-4060). The data was acquired with computer interfaced digital storage oscilloscope (Model Tektronix TDS2024). For Thermo-chromic analysis, each recorded texture was analyzed by using OLYSIA BIOREPORT software to determine red (R), green (G), blue (B) pixel value of an optical texture.

## 3. Results and Discussion

### 3.1 Thermally Switching

Temperature dependent morphology of PSCLC film was investigated through transmission mode based optical polarizing microscope, (setup shown in figure 1).

The oily streaks texture was observed in sample under crossed polarizer's when the liquid crystalline helix was confined with planer anchoring. In planer aligned cell with layers parallel to the conducting substrates, oily streaks appear as long bands that divide the ideal domains of liquid crystal molecules to form Grandjean polygenic texture as shown in Figure2(a-c).

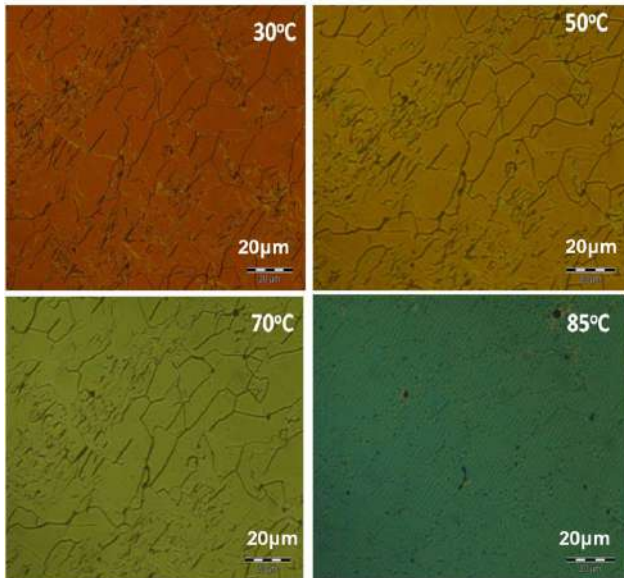


**Figure 2.** Morphology analysis through optical microscope under crossed polarizers at corresponding temperature (a). 30°C (b). 50°C (c). 70°C (d). 85°C respectively

As we raise the temperature from 30°C, selective reflections phenomenon occurs due to which change in color observed, which can be utilized for expanding thermo-chromism applications. This color change is due to the angular oscillations of liquid crystalline helix by providing thermal energy to LC molecules with raise in temperature. This phenomenon can be explained on the basis of theory of thermal expansion of liquid crystal, The Angular oscillations  $\langle \theta \rangle$  of liquid crystal can be defined mathematically<sup>[15]</sup> as

$$\langle \theta \rangle = \frac{AK_B T}{2I\omega^4} \quad (1)$$

Where  $K_B$  = Boltzmann constant,  $A$  = Anharmonicity coefficient,  $\omega$  = Angular frequency,  $I$  = Moment of inertia of molecules.

From equation 1, with raise in temperature, more is the angular oscillations and during the rotation of liquid crystalline molecules in the helix under the restriction of polymer network, selective color corresponds to characteristic wavelength is produced in Grandjean oily streak texture at a certain orientation. By attaining sufficient amount of thermal energy, these polygenic boundaries become unstable and start breaking with characteristic change in color of texture [Figure 2(c)]. The boundaries of these domains start disappear and start merging into each other's. While attaining the temperature 85°C, the transition of texture from oily streak Grandjean (polygenic) texture to under lying helix (ULH) texture was observed [Figure

2(d)] under crossed polarizer's. This ULH texture shows high thermal energy as compare to Grandjean texture (oily streak defects) as it appears at higher temperature. The fingerprint appears in ULH texture shows pitch of 0.8µm.

### 3.2 Thermo-chromic Responses

Figure 3 predicts the thermo-chromic response for the polymer stabilized liquid crystal textures at different temperature range.

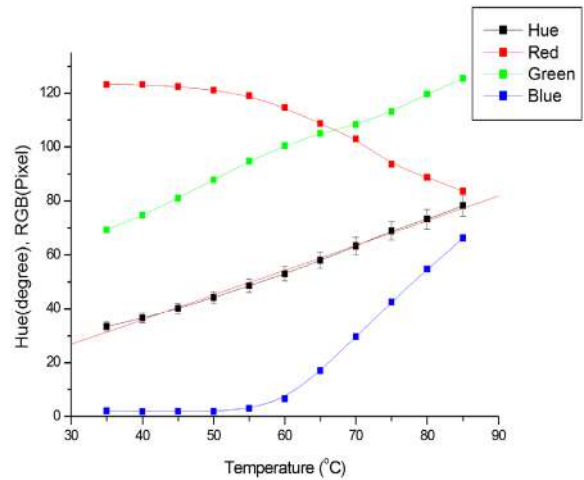


**Figure 3.** Temperature dependence of Hue and RGB variation for true color response.

We report here RGB pixel value and hue responses as a function of temperature for polymer stabilized textures for the purity of color, which is the combination of those characteristics of light that produce sensation of hue, saturation and intensity in normal human observer. Hue (H) gives the direct measure of color at which light emission from heat transfer surface occurs. With the help of OLYSIA BIOREPORT software, we have determined the value of RGB pixels and Hue response for different PSCLC textures taken from 35°C to 90°C temperature. After recording the Hue (H) values, it was fitted by equation<sup>[31]</sup>

$$H = \cos^{-1} \left| \frac{0.5 \times (R - G) + (R - B)}{(R - G)^2 + (R - B)(G - B)^{0.5}} \right| \quad (2)$$

Here R, G, B is value of red, green, blue respectively, which is getting record from OLYSIA software. Figure 3 represent the linear behavior of hue versus temperature in the range 35°C to 85°C, which is useful scale for the application of PSCLC sample as thermal imaging sensor.

### 4. Conclusion

In summary, we conclude that the morphology of PSCT textures show temperature dependence and gives appear-

ance of characteristic color as temperature is raised from 30°C. Therefore it can be used in thermal imaging. Also their responses can be engineered to accurate temperatures, but their color range is limited by their principle of operation and followed by linear behavior of hue in the specific range of temperature. Hence this PSCLC film can also worked as temperature indicators that modify the incident white light and display color whose wavelength is proportional to temperature.

## References

- [1] Hongwen Ren and Shin-Tson We, "Reflective reversed mode polymer stabilized cholesteric texture light switches", *J.Appl.Phys.* 2002, 92: 797.
- [2] J.W. Doane, N.A. Voz, B.-G. Wu, and S. Zumer, "Field controlled scattering from nematic microdroplets" *Appl. Phys. Lett.* 1986, 48: 269.
- [3] Ji Ma, Lei Shi and Deng ka Yang, "Bistable polymer stabilized cholesteric texture light shutter" *Appl. Phys. Express*, 2010, 3: 021702.
- [4] R. Bao, C.-M. Liu, and D.-K. Yang, "Smart bistable polymer stabilized cholesteric texture light shutter" *Appl. Phys. Express*, 2009, 2: 112401.
- [5] P.P. Crooker and D.K. Yang, "Polymer dispersed chiral liquid crystal color display" *Appl. Phys. Lett.* 1990, 57: 2529.
- [6] K. Kato, K. Tanaka, S. Tsuru and S. Sakai, "Reflective color display using polymer dispersed cholesteric liquid crystal.", *Jpn. J. Appl. Phys.* 1994, 33: 2635-2640.
- [7] H.-H. Liang, C.-C. Wu, P.-H. Wang, J.-Y. Lee, "Electro-thermal switchable bistable reverse mode polymer stabilized cholesteric texture light shutter", *Opt. Mater.* 2011, 33: 1195-1202.
- [8] Friedel, G., *Les états mésomorphes de la matière*, "Annl. Phys. 1922, 18: 273.
- [9] C.-Y. Huang, S. -Weike, Y.-S. Chih, "Electro-optical performance of Polymer Stabilized Cholesteric texture cell: the influence of chiral dopent and monomer concentration", *Optics Communications*, 2006, 266: 198-202.
- [10] J.B. Guo, H. Yang, R. Li, N. Ji, X. Dong, H. Wu, J. Wei," Effect of network conc. On the performance of Polymer stabilized cholesteric liquid crystal with double handed circularly polarized light reflection band", *J. Phys. Chem.C*, 2009, 113: 16538-16543.
- [11] S.W. Kang, S. Sprunt and L.C. Chien, "Structure and morphology of polymer stabilized cholesteric diffraction gratings" *Appl. Phys. Lett.* 2000, 76: 3516.
- [12] S.H. Kim, L.-C. Chien and L. Komitov, "Short pitch cholesteric electro-optical device stabilized by non uniform polymer network", *Appl. Phys. Lett.* 2005, 86: 161118.
- [13] I. Dierking,"Recent development in polymer stabilized liquid crystal", *Polym. Chem.* 2010, 1: 1153-59.
- [14] J. Guo, H. Wu, F. Chen, L. Zhang, W. He, H. Yang and J. Wei," Fabrication of multi-pitched photonic structure in cholesteric liquid crystal based on polymer template with helical structure", *J. Mater. Chem.* 2010, 20: 4094-4102.
- [15] P.S. Drazic, "Liquid Crystal Dispersion" World Scientific Singapore, 1995.
- [16] R. Kumar; K.K. Raina; "Electrically modulated fluorescence in optically active polymer stabilised cholesteric liquid crystal shutter" *Liquid Crystals*, 2014, 41: 228-233.
- [17] K.K. Raina and P. Kumar, "Polymer dispersed liquid crystal composite films-deoplet orientation and optical response." *Journal of the Indian Institute of Science*, 2009, 89: 243-248.
- [18] S.-Y. Lua and L.-C. Chien, "A polymer stabilized single layer color cholesteric liquid crystal display with anisotropic reflection." *Applied physics letters*, 2007, 91: 131119.
- [19] Rui Bao, Cheng-Mei Liu and Deng-Ke Yang, "Smart Bistable Polymer Stabilized Cholesteric Texture Light Shutter" *Applied Physics Express*, 2009, 2: 112401.
- [20] S. Wang, J. He, Y. Zeng, B. Yan, Y. Wang, "Effect of polymer structures on electro-optical properties of polymer stabilized liquid crystal films" *Front. Chem. Eng. China*, 2008, 2: 265-268.
- [21] C. V. Rajaram, S. D.Hudson, L. C. Chien, "Morphology of polymer stabilized liquid crystal" *Chem. Mater.* 1995, 7: 2300-2308.
- [22] E.Merck, Data sheet.
- [23] Norland, N.J., USA, Data sheet.
- [24] D.K. Yang and S.T. Wu; "Fundamentals of liquid crystal devices ( New York: John Wiley and Sons Inc)
- [25] G. Diankov, H. Naradikian and T. Angelov, Polymer-stabilized liquid crystal indicator used in thermometry, *J. Mater. Sci.: Mater. Electron*, 2003, 14: 831-832.
- [26] H. Guillard, P. Sixou, L. Reboul, A. Perichaud; "Electrooptical characterization of polymer stabilized cholesteric liquid crystals" *Polymer*, 2001, 42: 9753-9762.
- [27] X.T. Yahn, H. Cao, Z. Yang, H. Yang; "A selective reflecting film with a temperature-dependent pitch length." *Chienese chemical letters*, 2010, 2: 279-282.
- [28] S. Chandrashekar, *Liquid Crystal 2nd Edn.*, Cam-

- bridge University Press, Singapore, 1992.
- [29] Kumar, R., Raina, K.K., “Optical and electrical control of circularly polarised fluorescence in CdSe quantum dots dispersed polymer stabilised cholesteric liquid crystal shutter,” *Liquid Crystals*, 2016, 43: 994-1001.
- [30] Middha, M., Kumar, R., Raina, K.K., “Effects of chirality on optical and electro-optic behavior of nematic liquid crystals doped with functionalized silver nanoparticles,” *Journal of Molecular Liquids*, 2016, 219: 631-636.
- [31] J. Stasięka, A. Stasięka, M. Jewartowski, M.W. Collins, “Liquid crystal thermography and true-colour digital image processing” *Optics & Laser Technology*, 2006, 38: 243–256.

**REVIEW**

# Cellulose Acetate Reverse Osmosis Membranes for Desalination: A Short Review

Shuo Liu Lifen Hu Weicai Zhang Hongyang Ma\*

College of Materials Science and Engineering, Beijing University of Chemical Technology, Beijing, 100029, China

## ARTICLE INFO

*Article history*

Received: 20 August 2019

Accepted: 22 October 2019

Published Online: 30 October 2019

*Keywords:*

Cellulose acetate

Reverse osmosis membrane

Composition

Desalination

## ABSTRACT

Freshwater scarcity is a critical challenge that human society has to face in the 21<sup>st</sup> century. Desalination of seawater by reverse osmosis (RO) membranes was regarded as the most promising technology to overcome the challenge given that plenty of potential fresh water resources in oceans. However, the requirements for high desalination efficiency in terms of permeation flux and rejection rate become the bottle-neck which needs to be broken down by developing novel RO membranes with new structure and composition. Cellulose acetate RO membranes exhibited long durability, chlorine resistance, and outstanding desalination efficiency that are worthy of being recalled to address the current shortcomings brought by polyamide RO membranes. In terms of performance enhancement, it is also important to use new ideas and to develop new strategies to modify cellulose acetate RO membranes in response to those complex challenges. Therefore, we focused on the state of the art cellulose acetate RO membranes and discussed the strategies on membrane structural manipulation adjusted by either phase separation or additives, which offered anti-fouling, anti-bacterial, anti-chlorine, durability, and thermo-mechanical properties to the modified membranes associated with the desalination performance, i.e., permeation flux and rejection rate. The relationship between membrane structure and desalination efficiency was investigated and established to guide the development of cellulose acetate RO membranes for desalination.

## 1. Introduction

In the 21st century, due to climate change and further population growth, the world will be facing increasing pressures on energy and water shortages<sup>[1,2]</sup>. Successful scientific and technological attempts to address these two shortages, especially freshwater scarcity, can also contribute toward helpful solutions on a global scale<sup>[3]</sup>. Two strategies were implemented: one is to remediate the contaminated freshwater by means of environmental protection<sup>[4-6]</sup>, the other is to desalinate saline water,

e.g., brackish water and seawater, to achieve freshwater from ocean resources which are regarded as great and inexhaustible<sup>[7]</sup>. Therefore, direct distillation and reverse osmosis (RO) membrane technologies are the major approaches to obtain freshwater from saline water currently<sup>[2,8,9]</sup>. Considering huge energy assumption of the direct distillation, RO membrane technology is the most popular approach to gain freshwater, and 44 % of global freshwater by desalination was from RO plants<sup>[8]</sup>. In the 60s and 70s of last century, two types of RO membranes, cellulose

\*Corresponding Author:

Hongyang Ma,

College of Materials Science and Engineering, Beijing University of Chemical Technology, Beijing, 100029, China;

Email: mahy@mail.buct.edu.cn

acetate-based membrane and polyamide-based thin-film composite (TFC) membrane, were developed rapidly and dominated all markets for desalination<sup>[10]</sup>. Although the polyamide-based TFC membrane exhibited relatively high permeation flux and became the mainstream currently in desalination, however, cellulose acetate membrane with higher chlorine-resistance, high rejection rate and high durability that is unique and irreplaceable in seawater desalination industry<sup>[7]</sup>.

Cellulose acetate RO membrane exhibited asymmetrical structure, as shown in Figure 1<sup>[8]</sup>.

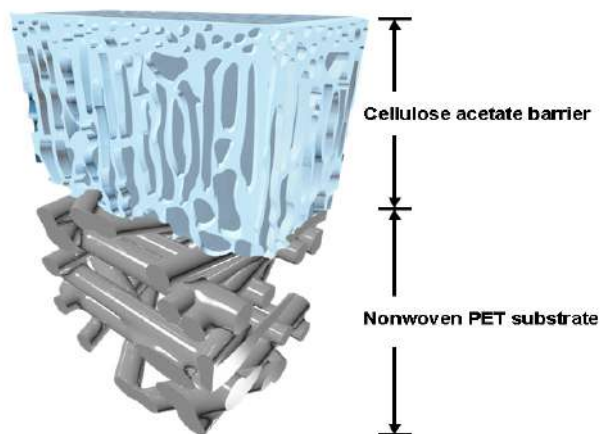


**Figure 1.** Representative structure of cellulose acetate RO membrane

Typically, the bottom layer of the RO membrane is polyester (e.g., polyethylene terephthalate, PET) non-woven substrate which mainly provided enough mechanical properties to the membrane; the middle and top layers are cellulose acetate fabricated by different approaches. The middle porous structure was created by phase-inversion method, where non-solvent induced a phase separation of cellulose acetate and extracted solvent (solvents) from cellulose acetate solution, and finger-shaped voids were formed after annealing treatment. The top skin layer of cellulose acetate membrane was generated by solvent evaporation and a non-porous dense layer was created for the selective separation of water molecules and sodium/chloride ions<sup>[8]</sup>. The top barrier layer and middle porous support layer are well integrated, together with PET non-woven mat to establish a cellulose acetate RO membrane for desalination.

Currently, the major challenge for cellulose acetate RO membrane remained was water permeation flux that needs to be enhanced to meet the requirement for desalination<sup>[11]</sup>. Every effort was made to address the problem by either adjusting the porous structure of the membrane by controlling the solvent-nonsolvent induced phase separation or creating nanocomposite top and middle layer by

forming additive-blending fabrication<sup>[12-17]</sup>. In addition to improve the permeation flux and rejection rate, cellulose acetate RO membranes with designed structure also exhibited highly improved anti-fouling<sup>[18-27]</sup>, anti-bacterial<sup>[28-38]</sup>, anti-chlorine<sup>[30,39]</sup>, and thermos-mechanical properties<sup>[40-49]</sup> that were benefit to enhance the desalination performance of the membranes, which was the main topic of the review.

## 2. Solvent-nonsolvent Induced Phase-inversion

Cellulose acetate RO membrane fabricated by phase-inversion method was firstly demonstrated by Loeb and Sourirajan<sup>[50]</sup> who employed cellulose acetate as the membrane material, and used formamide-acetone as the solvent and water as the nonsolvent, respectively. The phase separation behavior of the membrane preparation process was analyzed essentially by Strathmann<sup>[51]</sup>. The phase-separation diagram of cellulose acetate-formamide-acetone-water system was typically as shown in Figure 2.

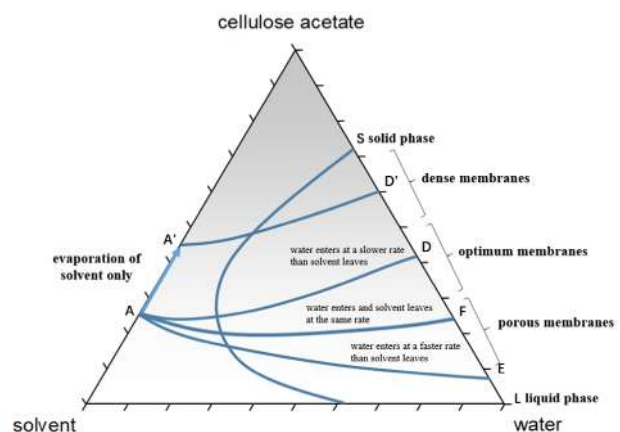


**Figure 2.** Phase diagram of the system acetate-formamide-acetone-water<sup>[51]</sup>

It was clear to see that the structure of the top barrier layer and middle layer of cellulose acetate was established by the evaporation of solvent and exchange rate of solvent and nonsolvent, respectively. Therefore, the cellulose acetate RO membrane could be designed by following the phase diagram for different applications, emphasized on either high rejection rate or high permeation flux. Moreover, change the solvent and nonsolvent compositions could further expanded the categories of cellulose acetate RO membrane. Pilon et. al.<sup>[52]</sup> adjust the ratio of solvent and nonsolvent to lower the operating pressure and to obtain the corresponding RO membrane with high permeation flux as 7.79 L/m<sup>2</sup>h while remaining the rejection rate of 95.0 %. Ghosh et. al. also partially change the solvent

of acetone to dioxane, and found that the permeate flux reached 10.78 L/m<sup>2</sup>h at 17.2 bar with 90.0 % rejection [53]. In Choi's work [12], with the increase of dioxane percentage, pure water flux of membranes goes up. Considering salt rejection rate, the optimal volume ratio of acetone/dioxane is 1:2.9. Moreover, Manjikian et al. used tetrahydrofurfuryl phosphate instead of formamide as non-solvent to fabricate RO membrane [54], where they found that the permeation flux and rejection rate increased. The research also investigated the optimum acetone-formamide range for RO membranes. By changing acetone/water ratio, Kunst [55] developed a relatively low pressure RO membrane casting solution composition at 90 % level of salt rejection rate.

To overcome the biological attack and the compaction problem, cellulose diacetate (CDA), cellulose triacetate (CTA), and their blends were suggested for RO membrane fabrication [10]. Ebrahim et. al. used the mixture of CA and CTA extracted from Egyptian rice straw [56] as the barrier layer and the resultant RO membrane exhibited high permeation flux of 4.76 L/m<sup>2</sup>h at 14 bar and rejection rate of 93.3 %. Meanwhile, CTA was introduced onto RO membrane barrier layer as the dense composition, while the CTA-CA membrane improved the permeation flux from 4.56 to 5.44 L/m<sup>2</sup>h and the rejection rate of the membrane up to 82.74 % [57].

In addition to factors mentioned above, annealing temperature and evaporation time were also important to

control the structure of cellulose acetate barrier layer, and therefore, improve the rejection rate of the membrane. Duarte et al. studied the effect of annealing temperature on CA-CTA membranes [58] and they found that the rejection rate increase with the annealing temperature rises up to 85 °C. Further temperature rise will drastically decrease the flux with relatively same rejection rate. Moreover, Manjikian et al. [54] changed the evaporation time from 0.25 to 3.0 min, and the rejection rate of the membrane increased at first and then decreased after the optimum evaporation time passed. Pageau [59] also investigated the effect of solvent evaporation time from 0.5 to 3.0 min: the permeate flux slightly increased within 1.0 min of evaporation, longer minutes of evaporation will cause a significant flux drop.

In summary, the dense barrier layer of cellulose acetate RO membrane was controlled by evaporation of solvent, such as acetone, and a phase inversion process. The barrier layer could be even denser by incorporation of dioxane, or involving other component, such as CTA. However, porous middle layer was mainly adjusted by the ratio of solvent-nonsolvent where increased non-solvent, e.g., water, will lead to larger pore size of the middle support. Meanwhile, change of the solvent and nonsolvent to dioxane can further improve the water permeability. The effects of parameters including barrier layer composition, solvent, nonsolvent, annealing conditions on the permeation flux (normalized by pressure) and rejection were illustrated in Table 1.

**Table 1.** Fabrication and performance of cellulose acetate RO membranes

Membrane	Composition of barrier	Solvent	Nonsolvent	Evaporation-time (min)	Annealing temperature (°C)	Permeation flux (LMH/bar)	Rejection (%)	Ref
Batch 18	CA	acetone	magnesium perchlorate solution	4.0	23.0-25.0	0.39	91.7	[60]
Batch 301				2.0	Pure water Pressure treatment	0.38	97.3	
Batch 47	CA	acetone	formamide	0.5-1.0	80.0	0.22	97.5	
				0.5	81.0	0.17	98.3	
S-2	CA	acetone+ dioxane	formamide	2.1×10 <sup>-3</sup>	81.0	0.56	90.0	[53]
					71.6	0.67	87.1	
	CA	acetone	THFP	10.0	75.0	0.21	96.5	[54]
			DMF	3.5	60.0	0.077	94.0	
			DMSO	3.0	62.0	0.071	85.0	
			urea solution	6.0	63.3	0.037	92.5	
			glyoxal solution	17.0	70.3	0.27	92.5	
			TEP	2.0	79.0	0.28	95.9	
			acetic acid	2.0	77.5	0.071	85.0	
optimized formulation	CA+CTA	acetone+ dioxane+ acetic acid	methanol	0.5	80.0-85.0	0.68	82.7	[61]
	CTA	acetone+ dioxane	methanol	1.5	without annealing	0.38	97.3	[62]
			maleic anhydride			0.12	96.5	

**Note:** DMF denotes dimethyl formamide  
 DMSO denotes dimethyl sulphoxide  
 TEP denotes triethyl phosphate  
 NM2P denotes N-methyl-2-pyrrolidone

Conventional cellulose acetate RO membranes developed since 60's last century and dominated major market for desalination based on the continuous optimization of the membrane structure and composition. However, the demanding of how to break through the flux limitation of current cellulose acetate RO membrane was still remained as a challenge, due to the increased human society's needs. Moreover, the trade-off between the permeation flux and rejection rate needs to be overcome in such a way that a membrane with high flux and high rejection rate will be required simultaneously. Fortunately, new nanoscaled materials such as nanoparticles, nanofibers, and nanofillers inspired a new pathway to improve the performance of the RO membranes.

### 3. Additives-based Nanocomposite

Nanoscaled materials, such as nanoparticles, nanofibers, nanotubes, and even 2D-nanosheets, can be integrated with cellulose acetate to form nanocomposite which may serve as barrier later and middle support layer for RO membranes [4]. The cellulose acetate nanocomposite RO membranes offer unique properties to the membrane, such as anti-fouling, anti-bacterial, anti-chlorine, high thermo-mechanical properties which all associated with improvement of the permeation flux and/or rejection rate in the desalination process [63]. Moreover, these nanoscaled additives may also change the structure of cellulose acetate by formation of water channels [64] for water molecule's transportation which directly induce high permeability of the membrane [65], as shown in Figure 3.

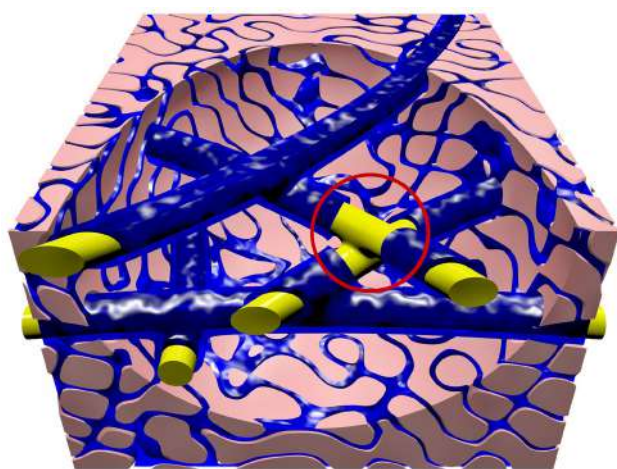


**Figure 3.** Schematic representation of the nature of water channels in the nanocomposite barrier layer [64]

Cellulose nanofibers were overlapped to form a 3D networks which serve as directed water channels (blue) formed by the connected tubular structure between the nanofibers and the polymer matrix (pink). The cut-out

in the red circle sketches the cross-linked nature of the nanofiber interconnects. Molecular cavities in the polymer matrix, as shown in Figure 3, which also contribute to the overall water flow through the barrier layer. Therefore, different types of nano-additives were embedded into cellulose acetate polymer matrix to enhance the membrane performance for desalination.

### 3.1 Anti-bacterial Properties

Typically, inorganic nanoparticles including Ag, ZnO, TiO<sub>2</sub>, hydroxyapatite, and bio-organic species such as chitosan, as well as ammonium- and bromo-modification of cellulose acetate issued anti-bacterial properties to the RO membranes.

According to Gul's work [66], when blending silver nitrate into CA/PEG casting solution, the fabricated membranes presented improved flux (0.31 L/m<sup>2</sup>h), salt rejection (94.5 %) and anti-E. coli properties. Similar results were proved by TiO<sub>2</sub> modified membranes with 95.4 % salt rejection [67]. Sprick et al. [68] introduced casein-coated Ag nanoparticles into cellulose acetate and fabricated RO membranes by physical blending and chemical attachment approach, the latter casted membrane exhibited 2.6 times higher rejection rate than pristine membrane without adding Ag. Moreover, when CA membranes were modified with silver nitrate by in-situ reduction [13], the flux increased from 0.80 to 0.95 L/m<sup>2</sup>h with relatively high salt rejection rate of 95.8 % compared with pristine membranes. The modified membranes also exhibit antibacterial activity against E. coli and B. subtilis. A new composite membrane containing cellulose acetate / graphene / Ag nanoparticles / Cu nanorods (CA-G-Ag-Cu) has been employed [69] to kill both Gram-positive and Gram-negative bacteria growth; meanwhile, both flux and salt rejection rate improvement were observed in permeability tests. Faria et al. [70] employed GO nanosheets and Ag nanoparticles to further improve anti-bacterial properties of the membrane. As a result, the integrated GO-silver nanoparticles-CA membranes own a high rejection rate of 90 % against E. coli. In addition to Ag, ZnO nanoparticles were also used to enhance anti-bacterial properties of cellulose acetate RO membrane. Khan et. al. [14] dispersed ZnO nanofillers in CA matrix and they found that fabricated membranes have a high Fe<sup>2+</sup> uptake capacity. Further permeability results suggest that the membranes may be suitable for water treatments. According to Ohland's work [71], incorporation of hydroxyapatite (Hap) into CA membranes by plasma treatment caused permeation flux increase from 5.85 to 7.65 L/m<sup>2</sup>h while high rejection of NaCl still remains. In Fei's work [72], surface modified CTA-RO membranes with 3-chloro-2-hydroxypro-

pyl-trimethyl ammonium chloride (CHPTAC) showed salt rejection rate of higher than 92 % with slight increase in flux and high bactericidal rates.

When antibacterial alkyl bromide modified CDA powder was used as the casting polymer<sup>[73]</sup>, both flux and rejection rate can reach up to the CTA-RO membrane. This new method of modification offers a new way for antibacterial improvements of CA membranes. Further improvement by introducing both quaternary ammonium and bromoacetyl groups<sup>[74]</sup> to CDA has shown bactericidal rates against *E. coli* and *S. aureus* more than 99.9 %. In addition, salt rejection and permeate flux are high with 96.76 % and 17.41 L/m<sup>2</sup>h, respectively.

### 3.2 Anti-fouling Properties

Hydrophilic species such as graphene oxide (GO), hydrophilic polymers, and surface-grafting with hydrophilic species may decrease surface tension and therefore offer anti-fouling properties to the membrane. Ahmad et. al.<sup>[75]</sup> employed silica into PEG/CA membranes, it turned out that not only the fouling resistance enhanced, but also was tested a 11 % increase in salt rejection up to 92.0 %. Meanwhile, permeate flux also increased from 0.35 to 2.46 L/m<sup>2</sup>h. When blending with CA, polyvinylchloride (PVC) modified RO membranes<sup>[15]</sup> also provided high salt rejection (93.3 %) and permeate flux of 13 L/m<sup>2</sup>h. The foulants rejection rate ranked 96.0-99.2 %. A composite CA membrane containing graphene, Ag nanoparticles and Cu nanorods<sup>[69]</sup> shown improved membrane desalination and biofouling properties simultaneously compared with neat CA membranes. Chemical attachment of silver nanoparticles/CA membranes in Sprick's study<sup>[68]</sup> have successfully prevented leaching of silver nanoparticles with better salt rejection and antimicrobial properties than conventional physical blending ones<sup>[76]</sup>.

The improvement of membrane hydrophilicity is a potential advantage over anti-protein and hydrophilic foulants. According to Morsy's study<sup>[77]</sup>, surface grafting of 2-acrylamido-2-methylpropanesulfonic acid (AMP-SA) suggested an increase in surface hydrophilicity with high salt rejection of 99.03 % and 6.00 L/m<sup>2</sup>h of flux. In Chen's research<sup>[65]</sup>, graphene oxide (GO) embedded CTA flat sheet membrane exhibit higher hydrophilic property with increased flux from 1.67 to 4.74 L/m<sup>2</sup>h. Simultaneously, salt rejection rate decrease at the same time which may due to the cause of internal water channels formation allowing passage of water and salt. Similar conclusions were also drawn in Shi's work<sup>[16]</sup> when it comes to GO-CA membrane.

In terms of surface modification, surface-initiated polymerization of 2-hydroxyethyl methacrylate (pHEMA)

reported by Worthley<sup>[78]</sup> had a 24 % improvement in resistance to seawater biofouling with only 6 % decrease in salt rejection and water flux. Instead of modification of CA-RO membranes to enhance anti fouling property, Sachit<sup>[79]</sup> suggested that pretreatment of feed water by ultrafiltration for improving the fouling problem should also be noted.

### 3.3 Anti-chlorine Properties

The addition of CNT can improve the chlorine resistance of cellulose acetate RO membranes. Wasim et. al.<sup>[39]</sup> incorporated sepiolite and polyvinylpyrrolidone (PVP) into cellulose acetate membrane which presented high NaCl and MgSO<sub>4</sub> rejection rate of 94 % and 92 % respectively after 2 hours of chlorination. Shafiq et. al.<sup>[67]</sup> employed TiO<sub>2</sub> nanoparticles to enhance anti-chlorine properties of the membrane and they found that the presence of TiO<sub>2</sub> exhibit negligible decline in salt rejection, with 15wt % of TiO<sub>2</sub> provide high salt rejection rate of 95.4 %.

### 3.4 Improved Thermo- and Mechanical Properties

Nano-additives such as CNT, GO, and silica nanoparticles can also improve the thermos or mechanical properties of cellulose acetate RO membranes.

Generally, GO modified CA membranes<sup>[65,80]</sup> has shown improved thermal stability with increasing amount of GO which induced stronger interactions between nanosheets and cellulose acetate. Such conclusions are also been proved by polyvinylchloride (PVC) blend CA membranes<sup>[15,81,82]</sup>, both thermal and mechanical properties improved with high rejection rate and relatively high permeate flux. According to Sabir's study<sup>[83]</sup>, when blending surface engineered (SE) multi-walled carbon nanotubes (MWCNTs), modified CA membranes exhibited higher weight loss temperature indicating an improvement in thermal stability with more MWCNT content with corresponding salt rejection rate of 99.8 %. Mechanical stability increased with embedding of silica nanoparticles<sup>[75]</sup> in CA membranes from 1 to 4 % (w/v), the salt rejection and permeation flux also increased as mentioned before this section. Similar results showed the improvement in thermal properties<sup>[84]</sup> alongside with the maximum salt rejection of 95.0 %. In Sabir's work, both tensile strength and Young's modulus increase with more fumed silica particles<sup>[85]</sup> in RO membranes.

Besides, long-term filtration process can testify the stability of modifiers as well as durability of membranes' anti-fouling property<sup>[86]</sup>. It has been proved by Chede<sup>[76]</sup> that after 26 days of filtration, the salt rejection drop of ca-

sein-Ag CA (2.8 %) is smaller than plain CA membranes (18.2 %). The permeation flux decline was 18 % compared to other membranes. Such results indicate that the introduction of Ag nanoparticles in membrane structure was efficient and durable. PVC/CA membranes prepared by Gendi<sup>[81]</sup> were proved to be able to work for long hours without breaking. During the 36 days' durability test, the rejection rate remained at the level of 98 - 99 %, with permeation flux of 37.2 L/m<sup>2</sup>h.

### 3.5 Improved Permeability and Rejection Rate

Some additives, such as modified coal<sup>[87,88]</sup> can improve the permeation flux and rejection rate of the composite by simply blending with cellulose acetate. The composite membrane exhibited high flux of 38.70 L/m<sup>2</sup>h and high rejection rate of 94.0 %, compared with the pristine CA membrane. Besides, when 0.005 wt% GO was used as an additive in CA membranes<sup>[16]</sup>, the water flux reached 13.65 L/m<sup>2</sup>h, 2.3 times higher than pristine CA ones, with 82.03 % salt rejection rate. Meanwhile, by surface grafting of 2-acrylamido-2-methylpropanesulfonic acid (AMP-SA)<sup>[77]</sup>, CA-RO membranes reached higher rejection rate of 99.03 % and water flux of 6.00 L/m<sup>2</sup>h. Other surface grafting of 2-acrylamidopropane-2-methyl sulfonic acid<sup>[56]</sup> increased water flux from 4.76 to 8.30 L/m<sup>2</sup>h and rejection rate reached 93.5 %. In Perera's study<sup>[89]</sup>, by adjusting CA concentration together with swelling and annealing treatment, CA thin film composite's salt rejection reached 94.0 % without significant sacrifice of water flux.

All these cellulose acetate composite RO membranes demonstrate high permeation flux and high rejection rate due to the integration of additives, as summarized in Table 2.

**Table 2.** Modified CA-RO membranes with enhanced desalination efficiency

Membrane	Additives	Flux (LMH/bar)	Rejection (%)	Anti-bacteria	Anti-fouling	Anti-chlorine	Thermo-mechanical strength	Ref
1	PEG200 + SiO <sub>2</sub>	0.165	98.4				×	[85]
2	PEG300 + SiO <sub>2</sub>	0.4	95.0				×	[84]
3	PEG400 + TiO <sub>2</sub>	0.02	95.4	×		×	×	[67]
4	PEG400 + MWCNT	0.15	99.8				×	[83]
5	PEG600 + SiO <sub>2</sub>	3.22	92.0	×			×	[75]
6	PEG600 + Ag	0.06	94.5	×				[66]
7	PEG600 + AgNO <sub>3</sub>	0.15	95.8	×				[13]

8	PEG600 + MWCNT	0.15	99.8					×	[83]
9	Modified coal	0.22	94.0						[88]
10	MWCNT	2.32	90.6						[12]
11	Casein-Ag	1.44	93.0	×				×	[41]
12	Graphene oxide	2.6	90.0					×	[80]
13	Graphene + Ag-Cu	3.12	98.0	×					[69]
14	Modified coal	1.75	94.0						[88]
15	Grafting AMPS	0.59	93.5						[56]
16	Br-CA	0.81	95.6	×				×	[73]
17	PVC	0.93	99.0					×	[81]
18	PVC	0.43	93.3		×			×	[15]
19	PVP + sepiolite	4.99	98.3	×			×		[39]
20	Hapf	0.51	89.2						[71]
21	CHPTAC	2.28	92.0	×				×	[72]
22	DMOA	1.12	96.8	×				×	[74]
23	AMPSA	0.4	99.0						[77]

### 4. Conclusion and Perspective

Cellulose acetate RO membranes were fabricated by phase-inversion approach and employed to brackish water and seawater desalination to address the critical issue of scarcity freshwater in global scale. The generation mechanism of cellulose acetate top barrier layer and sub-porous support layer was discussed comprehensively based on phase separation diagram of cellulose acetate-formamide-acetone-water system. The structure of dense barrier and porous substrate could be controlled by fine-tuning the solvent-nonsolvent induced phase separation of cellulose acetate, where high permeability and high rejection rate of the RO membranes could be designed and fabricated for desalination performance. The birth of new nanoscaled materials, such as nanoparticles, nanofibers, nanotubes, and nanosheets would break up the bottle neck limit which is the trade-off relationship between membrane permeability and selectivity. In this case, the nanocomposite RO membranes with both high permeate flux and rejection rate could be prepared for energy saving efficient desalination. Moreover, the nanoscaled additives also offer anti-fouling, anti-bacterial, anti-chlorine properties with high thermo-mechanical strength of CA-RO membranes which are all beneficial in improving desalination performances.

However, the fundamental physics and chemistry principles behind membrane formation mechanisms need to be

further explored, especially for the purpose of overpass the trade-off between the permeation and rejection rate which hinders the development of RO membranes. Given that limitness needs and requirements in human's society, the revolution of industry and growth of population require creation of new concept RO membranes with high permeation flux, high rejection rate, high durability and low cost, which are the direction we should follow in desalination industry.

### Acknowledgement

This work was supported by the National Natural Science Foundation of China (51673011).

### References

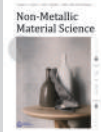
- [1] M. Qasim, M. Badrelzaman, N.N. Darwish, N.A. Darwish, N. Hilal, Reverse osmosis desalination: A state-of-the-art review, *Desalination*. 2019, 459: 59–104.  
DOI: 10.1016/j.desal.2019.02.008
- [2] M. Elimelech, W.A. Phillip, The Future of Seawater Desalination: Energy, Technology, and the Environment, *Science*. 2011, 333: 712–717.  
DOI: 10.1126/science.1200488
- [3] S.S. Shenvi, A.M. Isloor, A.F. Ismail, A review on RO membrane technology: Developments and challenges, *Desalination*. 2015, 368: 10–26.  
DOI: 10.1016/j.desal.2014.12.042
- [4] K.P. Lee, T.C. Arnot, D. Mattia, A review of reverse osmosis membrane materials for desalination—Development to date and future potential, *J. Membr. Sci.* 2011, 370: 1–22.  
DOI: 10.1016/j.memsci.2010.12.036
- [5] K.C. Khulbe, T. Matsuura, Recent Progresses in Preparation and Characterization of RO Membranes, *J. Membr. Sci. Res.*, 2016.  
DOI: 10.22079/jmsr.2016.22147
- [6] A. Giwa, N. Akther, V. Dufour, S.W. Hasan, A critical review on recent polymeric and nano-enhanced membranes for reverse osmosis, *RSC Adv.* 2016, 6: 8134–8163.  
DOI: 10.1039/C5RA17221G
- [7] M. Bassyouni, M.H. Abdel-Aziz, M.Sh. Zoromba, S.M.S. Abdel-Hamid, E. Drioli, A review of polymeric nanocomposite membranes for water purification, *J. Ind. Eng. Chem.* 2019, 73: 19–46.  
DOI: 10.1016/j.jiec.2019.01.045
- [8] H. Ma, B.S. Hsiao, Electrospun Nanofibrous Membranes for Desalination, in: *Curr. Trends Future Dev. Bio- Membr.*, Elsevier, 2019: 81–104.  
DOI: 10.1016/B978-0-12-813551-8.00004-8
- [9] S.S. Shenvi, A.M. Isloor, A.F. Ismail, A review on RO membrane technology: Developments and challenges, *Desalination*. 2015, 368: 10–26.  
DOI: 10.1016/j.desal.2014.12.042
- [10] S.S. Shenvi, A.M. Isloor, A.F. Ismail, A review on RO membrane technology: Developments and challenges, *Desalination*. 2015, 368: 10–26.  
DOI: 10.1016/j.desal.2014.12.042
- [11] M. Qasim, M. Badrelzaman, N.N. Darwish, N.A. Darwish, N. Hilal, Reverse osmosis desalination: A state-of-the-art review, *Desalination*. 2019, 459: 59–104.  
DOI: 10.1016/j.desal.2019.02.008
- [12] H. Choi, S.H. Yoon, M. Son, E. Celik, H. Park, H. Choi, Efficacy of synthesis conditions on functionalized carbon nanotube blended cellulose acetate membrane for desalination, *Desalination Water Treat.* 2016, 57: 7545–7554.  
DOI: 10.1080/19443994.2015.1025582
- [13] A. Ahmad, F. Jamshed, T. Riaz, S.- Gul, S. Waheed, A. Sabir, A.A. AlAnezi, M. Adrees, T. Jamil, Self-sterilized composite membranes of cellulose acetate/polyethylene glycol for water desalination, *Carbohydr. Polym.* 2016, 149: 207–216.  
DOI: 10.1016/j.carbpol.2016.04.104
- [14] S.B. Khan, K.A. Alamry, E.N. Bifari, A.M. Asiri, M. Yasir, L. Gzara, R.Z. Ahmad, Assessment of antibacterial cellulose nanocomposites for water permeability and salt rejection, *J. Ind. Eng. Chem.* 2015, 24: 266–275.  
DOI: 10.1016/j.jiec.2014.09.040
- [15] H. Abdallah, M.S. Shalaby, A. El-gendi, A.M. Shaban, B.-K. Zhu, Effectiveness of a coagulation step and polyester support on blend polyvinylchloride membrane formation and performance, *J. Polym. Eng.* 2019, 39: 351–359.  
DOI: 10.1515/polyeng-2018-0387
- [16] Y. Shi, C. Li, D. He, L. Shen, N. Bao, Preparation of graphene oxide–cellulose acetate nanocomposite membrane for high-flux desalination, *J. Mater. Sci.* 2017, 52: 13296–13306.  
DOI: 10.1007/s10853-017-1403-0
- [17] A. Ahmad, S. Waheed, S.M. Khan, S. e-Gul, M. Shafiq, M. Farooq, K. Sanauallah, T. Jamil, Effect of silica on the properties of cellulose acetate/polyethylene glycol membranes for reverse osmosis, *Desalination*. 2015, 355: 1–10.  
DOI: 10.1016/j.desal.2014.10.004
- [18] C. Sprick, S. Chede, V. Oyanedel-Craver, I.C. Escobar, Bio-inspired immobilization of casein-coated silver nanoparticles on cellulose acetate membranes for biofouling control, *J. Environ. Chem. Eng.* 2018, 6: 2480–2491.

- DOI: 10.1016/j.jece.2018.03.044
- [19] S. Chede, N.M. Anaya, V. Oyanedel-Craver, S. Gorgannejad, T.A.L. Harris, J. Al-Mallahi, M. Abu-Dalo, H.A. Qdais, I.C. Escobar, Desalination using low biofouling nanocomposite membranes: From batch-scale to continuous-scale membrane fabrication, *Desalination*. 2019, 451: 81–91.  
DOI: 10.1016/j.desal.2017.05.007
- [20] G. Kang, Y. Cao, Development of antifouling reverse osmosis membranes for water treatment: A review, *Water Res.* 2012, 46: 584–600.  
DOI: 10.1016/j.watres.2011.11.041
- [21] A. Ahmad, S. Waheed, S.M. Khan, S. e-Gul, M. Shafiq, M. Farooq, K. Sanullah, T. Jamil, Effect of silica on the properties of cellulose acetate/polyethylene glycol membranes for reverse osmosis, *Desalination*. 2015, 355:1–10.  
DOI: 10.1016/j.desal.2014.10.004
- [22] H. Abdallah, M.S. Shalaby, A. El-gendi, A.M. Shaban, B.-K. Zhu, Effectiveness of a coagulation step and polyester support on blend polyvinylchloride membrane formation and performance, *J. Polym. Eng.* 2019, 39: 351–359.  
DOI: 10.1515/polyeng-2018-0387
- [23] H. Choi, S.H. Yoon, M. Son, E. Celik, H. Park, H. Choi, Efficacy of synthesis conditions on functionalized carbon nanotube blended cellulose acetate membrane for desalination, *Desalination Water Treat.* 2016, 57: 7545–7554.  
DOI: 10.1080/19443994.2015.1025582
- [24] D. Sachit, J. Veenstra, Foulant Analysis of Three RO Membranes Used in Treating Simulated Brackish Water of the Iraqi Marshes, *Membranes*. 2017, 7: 23.  
DOI: 10.3390/membranes7020023
- [25] D.E. Abd-El-Khalek, B.A. Abd-El-Nabey, A. Morsy, Sh. Ebrahim, S.R. Ramadan Improvement of performance and antifouling properties of reverse osmosis membranes using green additive 65 71 10.5004/dwt.2019.23481, D.E. Abd-El-Khalek, B.A. Abd-El-Nabey, A. Morsy, Sh. Ebrahim, S.R. Ramadan, Improvement of performance and antifouling properties of reverse osmosis membranes using green additive, *DESALINATION WATER Treat.* 2019, 142: 65–71.  
DOI: 10.5004/dwt.2019.23481
- [26] C.H. Worthley, K.T. Constantopoulos, M. Ginic-Markovic, R.J. Pillar, J.G. Matisons, S. Clarke, Surface modification of commercial cellulose acetate membranes using surface-initiated polymerization of 2-hydroxyethyl methacrylate to improve membrane surface biofouling resistance, *J. Membr. Sci.* 2011, 385–386: 30–39.  
DOI: 10.1016/j.memsci.2011.09.017
- [27] A. El-Gendi, F.A. Samhan, N. Ismail, L.A.N. El-Dein, Synergistic role of Ag nanoparticles and Cu nanorods dispersed on graphene on membrane desalination and biofouling, *J. Ind. Eng. Chem.* 2018, 65: 127–136.  
DOI: 10.1016/j.jiec.2018.04.021
- [28] S.B. Khan, K.A. Alamry, E.N. Bifari, A.M. Asiri, M. Yasir, L. Gzara, R.Z. Ahmad, Assessment of antibacterial cellulose nanocomposites for water permeability and salt rejection, *J. Ind. Eng. Chem.* 2015, 24: 266–275.  
DOI: 10.1016/j.jiec.2014.09.040
- [29] C. Sprick, S. Chede, V. Oyanedel-Craver, I.C. Escobar, Bio-inspired immobilization of casein-coated silver nanoparticles on cellulose acetate membranes for biofouling control, *J. Environ. Chem. Eng.* 2018, 6: 2480–2491.  
DOI: 10.1016/j.jece.2018.03.044
- [30] M. Shafiq, A. Sabir, A. Islam, S.M. Khan, N. Gull, S.N. Hussain, M.T.Z. Butt, Cellulose acetate based thin film nanocomposite reverse osmosis membrane incorporated with TiO<sub>2</sub> nanoparticles for improved performance, *Carbohydr. Polym.* 2018, 186: 367–376.  
DOI: 10.1016/j.carbpol.2018.01.070
- [31] A.F. de Faria, A.C.M. de Moraes, P.F. Andrade, D.S. da Silva, M. do Carmo Gonçalves, O.L. Alves, Cellulose acetate membrane embedded with graphene oxide-silver nanocomposites and its ability to suppress microbial proliferation, *Cellulose*. 2017, 24: 781–796.  
DOI: 10.1007/s10570-016-1140-6
- [32] S. Chede, N.M. Anaya, V. Oyanedel-Craver, S. Gorgannejad, T.A.L. Harris, J. Al-Mallahi, M. Abu-Dalo, H.A. Qdais, I.C. Escobar, Desalination using low biofouling nanocomposite membranes: From batch-scale to continuous-scale membrane fabrication, *Desalination*. 2019, 451: 81–91.  
DOI: 10.1016/j.desal.2017.05.007
- [33] P. Fei, L. Liao, J. Meng, B. Cheng, X. Hu, J. Song, Non-leaching antibacterial cellulose triacetate reverse osmosis membrane via covalent immobilization of quaternary ammonium cations, *Carbohydr. Polym.* 2018, 181: 1102–1111.  
DOI: 10.1016/j.carbpol.2017.11.036
- [34] A.L. Ohland, V.M.M. Salim, C.P. Borges, Plasma functionalized hydroxyapatite incorporated in membranes for improved performance of osmotic processes, *Desalination*. 2019, 452: 87–93.  
DOI: 10.1016/j.desal.2018.11.008
- [35] A. Ahmad, F. Jamshed, T. Riaz, S.- Gul, S. Waheed, A. Sabir, A.A. AlAnezi, M. Adrees, T. Jamil, Self-steril-

- ized composite membranes of cellulose acetate/polyethylene glycol for water desalination, *Carbohydr. Polym.* 2016, 149: 207–216.  
DOI: 10.1016/j.carbpol.2016.04.104
- [36] A. El-Gendi, F.A. Samhan, N. Ismail, L.A.N. El-Dein, Synergistic role of Ag nanoparticles and Cu nanorods dispersed on graphene on membrane desalination and biofouling, *J. Ind. Eng. Chem.* 2018, 65: 127–136.  
DOI: 10.1016/j.jiec.2018.04.021
- [37] P. Fei, L. Liao, J. Meng, B. Cheng, X. Hu, J. Song, Synthesis, characterization and antibacterial properties of reverse osmosis membranes from cellulose bromoacetate, *Cellulose.* 2018, 25: 5967–5984.  
DOI: 10.1007/s10570-018-1990-1
- [38] Sabad-e-Gul, S. Waheed, A. Ahmad, S.M. Khan, M. Hussain, T. Jamil, M. Zuber, Synthesis, characterization and permeation performance of cellulose acetate/polyethylene glycol-600 membranes loaded with silver particles for ultra low pressure reverse osmosis, *J. Taiwan Inst. Chem. Eng.* 2015, 57: 129–138.  
DOI: 10.1016/j.jtice.2015.05.024
- [39] M. Wasim, A. Sabir, M. Shafiq, A. Islam, T. Jamil, Preparation and characterization of composite membrane via layer by layer assembly for desalination, *Appl. Surf. Sci.* 2017, 396 : 259–268.  
DOI: 10.1016/j.apsusc.2016.10.098
- [40] A. Sabir, M. Shafiq, A. Islam, F. Jabeen, A. Shafeeq, A. Ahmad, M.T. Zahid Butt, K.I. Jacob, T. Jamil, Conjugation of silica nanoparticles with cellulose acetate / polyethylene glycol 300 membrane for reverse osmosis using MgSO<sub>4</sub> solution, *Carbohydr. Polym.* 2016, 136: 551–559.  
DOI: 10.1016/j.carbpol.2015.09.042
- [41] S. Chede, N.M. Anaya, V. Oyanedel-Craver, S. Gorgannejad, T.A.L. Harris, J. Al-Mallahi, M. Abu-Dalo, H.A. Qdais, I.C. Escobar, Desalination using low biofouling nanocomposite membranes: From batch-scale to continuous-scale membrane fabrication, *Desalination.* 2019, 451: 81–91.  
DOI: 10.1016/j.desal.2017.05.007
- [42] S.M. Ghaseminezhad, M. Barikani, M. Salehirad, Development of graphene oxide-cellulose acetate nanocomposite reverse osmosis membrane for seawater desalination, *Compos. Part B Eng.* 2019, 161: 320–327.  
DOI: 10.1016/j.compositesb.2018.10.079
- [43] A. Ahmad, S. Waheed, S.M. Khan, S. e-Gul, M. Shafiq, M. Farooq, K. Sanaulah, T. Jamil, Effect of silica on the properties of cellulose acetate/polyethylene glycol membranes for reverse osmosis, *Desalination.* 2015, 355: 1–10.  
DOI: 10.1016/j.desal.2014.10.004
- [44] H. Abdallah, M.S. Shalaby, A. El-gendi, A.M. Shaban, B.-K. Zhu, Effectiveness of a coagulation step and polyester support on blend polyvinylchloride membrane formation and performance, *J. Polym. Eng.* 2019, 39: 351–359.  
DOI: 10.1515/polyeng-2018-0387
- [45] K. Chen, C. Xiao, Q. Huang, H. Liu, Y. Tang, Fabrication and properties of graphene oxide-embedded cellulose triacetate RO composite membrane via melting method, *Desalination.* 2018, 425: 75–184.  
DOI: 10.1016/j.desal.2017.10.004
- [46] A. Sabir, M. Shafiq, A. Islam, A. Sarwar, M.R. Dilshad, A. Shafeeq, M.T. Zahid Butt, T. Jamil, Fabrication of tethered carbon nanotubes in cellulose acetate/polyethylene glycol-400 composite membranes for reverse osmosis, *Carbohydr. Polym.* 2015, 132: 589–597.  
DOI: 10.1016/j.carbpol.2015.06.035
- [47] H. Abdallah, A. El Gendi, M.S. Shalaby, A. Amin, M. El-Bayoumi, A.M. Shaban, Influence of cellulose acetate polymer proportion on the fabrication of polyvinylchloride reverse osmosis blend membrane, experimental design, *DESALINATION WATER Treat.* 2018, 116: 29–38.  
DOI: 10.5004/dwt.2018.22306
- [48] A. El-Gendi, H. Abdallah, A. Amin, S.K. Amin, Investigation of polyvinylchloride and cellulose acetate blend membranes for desalination, *J. Mol. Struct.* 2017, 1146: 14–22.  
DOI: 10.1016/j.molstruc.2017.05.122
- [49] A. Sabir, A. Islam, M. Shafiq, A. Shafeeq, M.T.Z. Butt, N.M. Ahmad, K. Sanaulah, T. Jamil, Novel polymer matrix composite membrane doped with fumed silica particles for reverse osmosis desalination, *Desalination.* 2015, 368: 159–170.  
DOI: 10.1016/j.desal.2014.12.041
- [50] S. Loeb, S. Sourirajan, Sea Water Demineralization by Means of an Osmotic Membrane, in: *Saline Water Conversion—II, AMERICAN CHEMICAL SOCIETY, WASHINGTON, D. C., 1963: 117–132.*  
DOI: 10.1021/ba-1963-0038.ch009
- [51] H. Strathmann, P. Scheible, R.W. Baker, A rationale for the preparation of Loeb-Sourirajan-type cellulose acetate membranes, *J. Appl. Polym. Sci.* 1971, 15: 811–828. DOI: 10.1002/app.1971.070150404
- [52] R. Pilon, B. Kunst, S. Sourirajan, Studies on the development of improved reverse osmosis membranes from cellulose acetate–acetone–formamide casting solutions, *J. Appl. Polym. Sci.* 1971, 15: 1317–1334.  
DOI: 10.1002/app.1971.070150603
- [53] A.K. Ghosh, K.K. Sirkar, Low-pressure reverse os-

- mosis desalination with improved cellulose acetate membranes, *J. Appl. Polym. Sci.* 1979, 23: 1291–1307.  
DOI: 10.1002/app.1979.070230503
- [54] S. Manjikian, Desalination Membranes from Organic Casting Solutions, *Ind. Eng. Chem. Prod. Res. Dev.* 1967, 6: 23–32.  
DOI: 10.1021/i360021a004
- [55] B. Kunst, S. Sourirajan, Development and performance of some porous cellulose acetate membranes for reverse osmosis desalination, *J. Appl. Polym. Sci.* 1970, 14: 2559–2568.  
DOI: 10.1002/app.1970.070141011
- [56] Sh. Ebrahim, A. Mosry, E. Kanawy, T. Abdel-Fattah, S. Kandil, Reverse osmosis membranes for water desalination based on cellulose acetate extracted from Egyptian rice straw, *Desalination Water Treat.* 2015: 1–11.  
DOI: 10.1080/19443994.2015.1110052
- [57] A.P. Duarte, M.T. Cidade, J.C. Bordado, Cellulose acetate reverse osmosis membranes: Optimization of the composition, *J. Appl. Polym. Sci.* 2006, 100: 4052–4058.  
DOI: 10.1002/app.23237
- [58] A.P. Duarte, J.C. Bordado, M.T. Cidade, Influence to the performance of cellulose acetate reverse osmosis membranes by fibers addition, *J. Appl. Polym. Sci.* 2008, 109: 2321–2328.  
DOI: 10.1002/app.28319
- [59] L. Pageau, S. Sourirajan, Improvement of porous cellulose acetate reverse osmosis membranes by change of casting conditions, *J. Appl. Polym. Sci.* 1972, 16: 3185–3206.  
DOI: 10.1002/app.1972.070161212
- [60] B. Kunst, S. Sourirajan, Performance of some improved porous cellulose acetate membranes for low pressure reverse osmosis desalination, *Desalination.* 1970, 8: 139–152.  
DOI: 10.1016/S0011-9164(00)82018-4
- [61] A.P. Duarte, J.C. Bordado, M.T. Cidade, Cellulose acetate reverse osmosis membranes: Optimization of preparation parameters, *J. Appl. Polym. Sci.* 2007, 103: 134–139.  
DOI: 10.1002/app.24837
- [62] J.D. Nirmal, V.P. Pandya, N.V. Desai, R. Rangarajan, Cellulose Triacetate Membrane for Applications in Plating, Fertilizer, and Textile Dye Industry Wastes, *Sep. Sci. Technol.* 1992, 27: 2083–2098.  
DOI: 10.1080/01496399208019467
- [63] H. Zhang, G.M. Geise, Modeling the water permeability and water/salt selectivity tradeoff in polymer membranes, *J. Membr. Sci.* 2016, 520: 790–800.  
DOI: 10.1016/j.memsci.2016.08.035
- [64] H. Ma, C. Burger, B.S. Hsiao, B. Chu, Highly Permeable Polymer Membranes Containing Directed Channels for Water Purification, *ACS Macro Lett.* 2012, 1: 723–726.  
DOI: 10.1021/mz300163h
- [65] K. Chen, C. Xiao, Q. Huang, H. Liu, Y. Tang, Fabrication and properties of graphene oxide-embedded cellulose triacetate RO composite membrane via melting method, *Desalination.* 2018, 425: 175–184.  
DOI: 10.1016/j.desal.2017.10.004
- [66] Sabad-e-Gul, S. Waheed, A. Ahmad, S.M. Khan, M. Hussain, T. Jamil, M. Zuber, Synthesis, characterization and permeation performance of cellulose acetate/polyethylene glycol-600 membranes loaded with silver particles for ultra low pressure reverse osmosis, *J. Taiwan Inst. Chem. Eng.* 2015, 57: 129–138.  
DOI: 10.1016/j.jtice.2015.05.024
- [67] M. Shafiq, A. Sabir, A. Islam, S.M. Khan, N. Gull, S.N. Hussain, M.T.Z. Butt, Cellulose acetate based thin film nanocomposite reverse osmosis membrane incorporated with TiO<sub>2</sub> nanoparticles for improved performance, *Carbohydr. Polym.* 2018, 186: 367–376.  
DOI: 10.1016/j.carbpol.2018.01.070
- [68] C. Sprick, S. Chede, V. Oyanedel-Craver, I.C. Escobar, Bio-inspired immobilization of casein-coated silver nanoparticles on cellulose acetate membranes for biofouling control, *J. Environ. Chem. Eng.* 2018, 6: 2480–2491.  
DOI: 10.1016/j.jece.2018.03.044
- [69] A. El-Gendi, F.A. Samhan, N. Ismail, L.A.N. El-Dein, Synergistic role of Ag nanoparticles and Cu nanorods dispersed on graphene on membrane desalination and biofouling, *J. Ind. Eng. Chem.* 2018, 65: 127–136.  
DOI: 10.1016/j.jiec.2018.04.021
- [70] A.F. de Faria, A.C.M. de Moraes, P.F. Andrade, D.S. da Silva, M. do Carmo Gonçalves, O.L. Alves, Cellulose acetate membrane embedded with graphene oxide-silver nanocomposites and its ability to suppress microbial proliferation, *Cellulose.* 2017, 24: 781–796.  
DOI: 10.1007/s10570-016-1140-6
- [71] A.L. Ohland, V.M.M. Salim, C.P. Borges, Plasma functionalized hydroxyapatite incorporated in membranes for improved performance of osmotic processes, *Desalination.* 2019, 452: 87–93.  
DOI: 10.1016/j.desal.2018.11.008
- [72] P. Fei, L. Liao, J. Meng, B. Cheng, X. Hu, J. Song, Non-leaching antibacterial cellulose triacetate reverse osmosis membrane via covalent immobilization of

- quaternary ammonium cations, *Carbohydr. Polym.* 2018, 181: 1102–1111.  
DOI: 10.1016/j.carbpol.2017.11.036
- [73] P. Fei, L. Liao, J. Meng, B. Cheng, X. Hu, J. Song, Synthesis, characterization and antibacterial properties of reverse osmosis membranes from cellulose bromoacetate, *Cellulose*. 2018, 25: 5967–5984.  
DOI: 10.1007/s10570-018-1990-1
- [74] F. Li, P. Fei, B. Cheng, J. Meng, L. Liao, Synthesis, characterization and excellent antibacterial property of cellulose acetate reverse osmosis membrane via a two-step reaction, *Carbohydr. Polym.* 216: 312–321.  
DOI: 10.1016/j.carbpol.2019.04.026
- [75] A. Ahmad, S. Waheed, S.M. Khan, S. e-Gul, M. Shafiq, M. Farooq, K. Sanauallah, T. Jamil, Effect of silica on the properties of cellulose acetate/polyethylene glycol membranes for reverse osmosis, *Desalination*. 2015, 355: 1–10.  
DOI: 10.1016/j.desal.2014.10.004
- [76] S. Chede, N.M. Anaya, V. Oyanedel-Craver, S. Gorgannejad, T.A.L. Harris, J. Al-Mallahi, M. Abu-Dalo, H.A. Qdais, I.C. Escobar, Desalination using low biofouling nanocomposite membranes: From batch-scale to continuous-scale membrane fabrication, *Desalination*. 2019, 451: 81–91.  
DOI: 10.1016/j.desal.2017.05.007
- [77] A. Morsy, S. Ebrahim, E.-R. Kenawy, T. Abdel-Fattah, S. Kandil, Grafted cellulose acetate reverse osmosis membrane using 2-acrylamido-2-methylpropanesulfonic acid for water desalination, *Water Sci. Technol. Water Supply*. 2016, 16: 1046–1056.  
DOI: 10.2166/ws.2016.025
- [78] C.H. Worthley, K.T. Constantopoulos, M. Ginic-Markovic, R.J. Pillar, J.G. Matison, S. Clarke, Surface modification of commercial cellulose acetate membranes using surface-initiated polymerization of 2-hydroxyethyl methacrylate to improve membrane surface biofouling resistance, *J. Membr. Sci.* 2011, 385–386: 30–39.  
DOI: 10.1016/j.memsci.2011.09.017
- [79] D. Sachit, J. Veenstra, Foulant Analysis of Three RO Membranes Used in Treating Simulated Brackish Water of the Iraqi Marshes, *Membranes*. 2017, 7: 23.  
DOI: 10.3390/membranes7020023
- [80] S.M. Ghaseminezhad, M. Barikani, M. Salehirad, Development of graphene oxide-cellulose acetate nanocomposite reverse osmosis membrane for seawater desalination, *Compos. Part B Eng.* 2019, 161: 320–327.  
DOI: 10.1016/j.compositesb.2018.10.079
- [81] A. El-Gendi, H. Abdallah, A. Amin, S.K. Amin, Investigation of polyvinylchloride and cellulose acetate blend membranes for desalination, *J. Mol. Struct.* 2017, 1146: 14–22.  
DOI: 10.1016/j.molstruc.2017.05.122
- [82] H. Abdallah, A. El Gendi, M.S. Shalaby, A. Amin, M. El-Bayoumi, A.M. Shaban, Influence of cellulose acetate polymer proportion on the fabrication of polyvinylchloride reverse osmosis blend membrane, experimental design, *Desalination and Water Treat.* 2018, 116: 29–38.  
DOI: 10.5004/dwt.2018.22306
- [83] A. Sabir, M. Shafiq, A. Islam, A. Sarwar, M.R. Dilshad, A. Shafeeq, M.T. Zahid Butt, T. Jamil, Fabrication of tethered carbon nanotubes in cellulose acetate/polyethylene glycol-400 composite membranes for reverse osmosis, *Carbohydr. Polym.* 2015, 132: 589–597.  
DOI: 10.1016/j.carbpol.2015.06.035
- [84] A. Sabir, M. Shafiq, A. Islam, F. Jabeen, A. Shafeeq, A. Ahmad, M.T. Zahid Butt, K.I. Jacob, T. Jamil, Conjugation of silica nanoparticles with cellulose acetate/polyethylene glycol 300 membrane for reverse osmosis using MgSO<sub>4</sub> solution, *Carbohydr. Polym.* 2016, 136: 551–559.  
DOI: 10.1016/j.carbpol.2015.09.042
- [85] A. Sabir, A. Islam, M. Shafiq, A. Shafeeq, M.T.Z. Butt, N.M. Ahmad, K. Sanauallah, T. Jamil, Novel polymer matrix composite membrane doped with fumed silica particles for reverse osmosis desalination, *Desalination*. 2015, 368: 159–170.  
DOI: 10.1016/j.desal.2014.12.041
- [86] G. Kang, Y. Cao, Development of antifouling reverse osmosis membranes for water treatment: A review, *Water Res.* 2012, 46: 584–600.  
DOI: 10.1016/j.watres.2011.11.041
- [87] B.S. Thaçi, S.T. Gashi, The Heterogeneous Reverse Osmosis Membranes Based Separation of Fluorides with Fly Ash Pretreatment, *Acta Phys. Pol. A.* 2015, 128: B-62-B-67.  
DOI: 10.12693/APhysPolA.128.B-62
- [88] B. Thaçi, S. Gashi, N. Daci, M. Daci, A. Dylhasi, Effect of modified coal through chemical activation process on performance of heterogeneous reverse osmosis membranes, *Environment Protection Engineering*, 2015, 14: 1.  
DOI: 10.5277/epe150105
- [89] D.H.N. Perera, S.K. Nataraj, N.M. Thomson, A. Sepe, S. Hüttner, U. Steiner, H. Qiblawey, E. Sivaniah, Room-temperature development of thin film composite reverse osmosis membranes from cellulose acetate with antibacterial properties, *J. Membr. Sci.* 2014, 453: 212–220.  
DOI: 10.1016/j.memsci.2013.10.062



## REVIEW

# A Parametric Approach to the Evaluation of Flexural Strength of Advanced Ceramic or Glass Like Cylindrical Rods at Ambient Temperature

**Padmanabhan Krishnan\***

Department of Manufacturing Engineering, School of Mechanical Engineering, VIT University, Vellore, 632014, India

### ARTICLE INFO

#### Article history

Received: 8 October 2019

Accepted: 22 October 2019

Published Online: 30 October 2019

#### Keywords:

Flexure strength

Ceramics

Glasses

Fracture

Surface Finish

Length to Diameter Ratio

Flaw size

Strain

### ABSTRACT

This critical review presents a parametric approach to the evaluation of flexural strength of advanced ceramic or glass like cylindrical rods at ambient temperature. The parameters governing the measurement and evaluation of flexure strengths of glasses and ceramics are detailed with references. The scope for improvement in the existing ASTM STM C -1684 standard is described with a logical rationale and the parameters that need to be addressed are listed and explained.

## 1. Introduction

A flexure test to measure and evaluate the strength of ceramics and glasses must have information on allowable porosities. Flaw levels in the cylindrical rod have to be prescribed for measurements sake, as there is severe emphasis in flexure testing on fracture and Weibull distributions. They depend a lot on porosity levels. When we mention whisker reinforced composites and their applicability to the testing procedures there must be a mention on whether they are random or aligned. Whisker reinforced ceramics can also be bi modular making it a

little easier for characterization. These composites cannot be isotropic if they are aligned. Randomness is closer to quasi-isotropy mostly. These issues have to be addressed if flexure testing is considered applicable to whisker reinforced composites as well. There has to be a realistic approach in the consideration of raw data and heat treated data for flaw reduction and porosity reduction as uniformity is achieved through heat treatment. The requirements and recommendations according to this publication can be followed that would make flexural strength testing more reliable and consistent.

\*Corresponding Author:

Padmanabhan Krishnan,

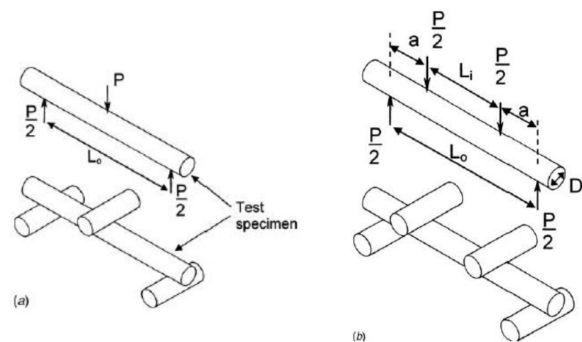
Department of Manufacturing Engineering, School of Mechanical Engineering, VIT University, Vellore, 632014, India;

Email: padmanabhan.k@vit.ac.in

## 2. Parametric Approach

Grinding is an operation meant to produce a surface finish of less than 2-3  $\mu\text{m}$ <sup>[1]</sup>. It is a final operation that hones a surface. As porosity is taken in to account by flexure testing procedures, there should be a table on the need for a surface finish of a required fine surface roughness finish. One cannot prescribe a uniform 600 grit finish surface as in some investigations<sup>[2]</sup>. As the natural flaw size vs. grinding damage size matters in flexure testing as governed by the findings of fracture mechanics, the surface flaw size should be lower than the critical crack length that is required for fracture. As we know about the critical flaw size required for fracture which depends on the critical stress intensity factor and the flaw size limit in order to get a particular stress value which is reported as strength. As flexure strength depends on the flaw size and  $K_{Ic}$  in tension, the critical flaw size for most ceramics and glasses are anywhere from submicron resolution to a few microns. Some glasses can have, say 0.8 microns of critical crack size above which fracture occurs<sup>[3]</sup>. The contention here is that by using a 600 grit finish, one is creating a 3-5 micron crack length on the surface (any machining company brochure will do to justify this statement on the  $R_{max}$  obtainable on a ceramic for a grit size with 25-28 micron sized ceramic particles or diamond particles)<sup>[4]</sup> of a glass like material which has a critical crack length of a micron or lower. So, for a class of glassy materials to be evaluated for their flexure strength, the surface finish must be finer than the critical crack length that is natural to them in bulk. Virtually for a ceramic surface, the use of Silicon carbide grits is difficult. Diamond or harder ceramic particles are more suitable. A standard practice must also make enough prescription for whisker reinforced composites or other Ceramic Matrix Composites (CMCs) that may have shorter or longer critical flaws. A finer prescription on the surface finish requirements will ensure that surface conditions do not reduce the flexural strength of a specimen. It should not be allowed play a dubious role based on the flaw size vs. surface damage condition ratios. 1500 grit finish or above would create a surface with an  $R_{max}$  of less than a micron which would fulfill the requirements for testing. The allowables for support span to diameter ratios to measure flexural strength are anywhere between 2.9 to 20 in the standard STM-C 1684 for flexure testing of ceramics published by an ASTM committee<sup>[2]</sup>. Sufficient knowledge of compression, tension and shear in ceramics and glasses will inform an evaluator that a fixed span to diameter ratio must be agreed upon by those concerned as all ASTM standards are voluntary consensus standards. Though, every materials engineer knows that

long beams provide a closer to the elastic modulus value and shorter beams provide a lower modulus, a fixed span has not been prescribed for the flexure tests of ceramics and glasses. As shorter beams have more shear component they would provide a higher flexural strength value than a longer span specimen with the same diameter. Considering that the tensile to compressive strength ratios of cylindrical rod like ceramics and glasses are in the range of say, 150/2000 MPa, the flexural strength is higher than the tensile strength but lower than the compressive strength. It has a dependence on the span to diameter ratio also. A common span must have been prescribed for a class of materials to regulate the repeatability within a laboratory and reproducibility between laboratories. The minimum span to diameter ratio of 3 prescribed for flexure testing of ceramic/ glass cylindrical rods at a small diameter would lead to a very low strength in the vicinity of surface flaws produced by a 600 grit finish and a higher strength when finished to a sub-micron resolution using a grit number like 1500. Besides, for a small cross section, the defect population is less and the flexural strength may be more subject to a good surface finish as mentioned before. However, for a larger specimen with a span to depth ratio of about 29, the flexural strength could be lower even for the same defect population as there are more defects across the cross section and along the length. Hence, at a nominal defect population for thicker and longer specimens which would be practically higher along and across the cross section, the flexure strength could be low. In the absence of flaws one might expect the size effect to take over and larger specimens might exhibit higher flexural strength even within the present domain. One must standardize on the span. Please see Figure 1 for a schematic understanding of the test dimensions.



**Figures 1 (a) and (b).** The load ( $P$ ), its distributions in the three (a) and four point (b) set up, the roller and specimen diameters and the support span lengths are marked

The effective area and effective volume calculations for test specimens concerned are not clearly spelt in the C 1684 standard for all the reasons described earlier here.

As there has been no clarity on porosities, scatter, span to diameter ratio and surface finish, any attempt to understand the variabilities in strength through statistical means is null and void. A statistical meaning would be justified only when a sound parametric approach is followed.

While discussing the crack growth rates that are important in ceramics, glasses and CMCs, the loading rates, constant cross head velocities or strain rates must be specified in a standard. A constant cross head velocity and a constant strain rate cannot be achieved simultaneously in the same test. Each one of them generates different crack growth rate(s) and fracture. Recommended constant strain rates or cross head velocities that generate an increasing strain rate as the sample nears fracture must be based on an understanding of strict domains of quasi-static or dynamic fracture. A constant cross head velocity value does not produce a constant strain rate nor can it be called one. An exponential decay of cross head velocity gives a constant strain rate when the exponent 'k' in the exponential term is adjusted to provide a constant strain rate<sup>[5]</sup>. Experiments on the DARTEC systems by Prof. YVRK Prasad and group may be referred to. It is very important to note that the conditions change with the length, diameter and span to depth ratio in order to maintain a range of increasing strain rates at a constant cross head velocity or a constant strain rate with an exponential decay of cross-head velocity. The standard C- 1684 prescribes a strain rate evaluation formulation based on a constant cross head velocity which is erroneous. It would have been better to prescribe one of the criteria mentioned above and not confuse the researchers.

The flexure strength is higher than the tensile strength for the span: diameter ratios used in the standard C 1684. Even if a single common span is used, the results will be likewise. However, the authors of C 1684 have made the statement 'tensile strength is measured using the flexure test' in the opening statement of their JTEVA paper<sup>[6]</sup>. (Journal of Testing and Evaluation, Vol. 37, No. 3 Paper ID JTE101649, by George D Quinn, Brian T Spareberg, Lewis K Ives, Said Jahanmir, Philip Koshy and Dwayne D Arola, on Flexural strength of glass and ceramic rods). Though the publication is by a National Institute of Standards and Technology group from Gaithersburg, USA, they have not referred to the other works from the same cradle that clearly give a lower tensile strength value to ceramics and glasses compared to their flexural strengths. It is known that it is difficult to do tensile tests for ceramics but any scaling done with the help of flexure tests must be based on sound logic. Any attempt of scaling done otherwise, will not be even precise with a margin of error, leave alone being accurate. As they say accuracy is being

bang on target and precision is how exactly far away you are from it. The JTEVA paper should have not made an opening statement on measuring tensile strength through flexure based on their given fallacies. Only flexure strength can be measured with flexure tests. Scaling must depend on size effects, span to depth/dia ratios, stress concentration effects at the roller sites, Weibull statistics and effective area and volume analyses based on the all of the above.

Further, the grain size conditions, processing history and heat treatment procedure requirements, if any, are never mentioned in the standard.

### 3. Casual Factors in Fracture

Some casual factors that arise in addition to the root causes in the failure of the C 1684 standard to hold itself together are the following:

(1) Rubber banding of the rollers alters the span to diameter ratio whilst the specimen is being tested. It is not a correct practice.

(2) The cradle material is not specified in the standard though it is a form of rubber. The user should not be made to guess.

(3) As flexure is compressive and tensile in a certain ratio, it is also end face dependent especially in solid cylindrical rods. The face ends on glasses, ceramics and CMCs, must have strict prescriptions on special machining of the ends. Cracks generate at the face ends due to shear and bending as the top of the specimen experiences compression and the bottom experiences tension, when bent from the top. The standard prescription for the cylindrical surface holds good for the end faces as well.

(4) No diameter tolerances have been specified for elliptical specimens which also form a part of the standard. (Like major axis and minor axis).

(5) A statement in the standard reads, 'Ave. stress less than 2.5 %' which is erroneous. The statement must be removed.

(6) Another statement reads, 'Strength to elastic modulus ratio of 1000'. Which can never be but only otherwise.

(7) The standard does not address stress concentration factors leading to fracture.

(8) Three point and four point bend test comparisons are not convincing in the standard.

(9) Valid vs. invalid failures have not been discussed properly or their outcomes and recommendations laid down properly. Some of the flaws in the standard that are pointed out here will help in clearing the picture.

(10) The NIST data that are freely available, list the tensile, flexural and compressive strengths of many ceramics and glasses. The flexural strength is always higher

than the tensile strength for these class of materials, much against the statement given in the JTEVA paper<sup>[6]</sup>.

(11) Materials like cubic boron nitride, tantalum carbide, hexaborides and the likes are advanced ceramics not alumina, SiC and the likes. Most of the data available and the test results available for the ceramics are those of basic ceramics and glasses. However, the title 'advanced ceramics' is cited in the standard for experimental work on basic ceramics.

Hence, in the author's opinion the standard STM C-1684 must be withdrawn by the persons who developed it and the committee that voted it in and revised for reconsideration. Outside experts in the field must be brought in to do a lot of work to turn this attempt in to success. After all, ASTM standards are voluntary consensus standards and should not be a product of oligarchy. A parametric approach should be followed based on a strong rationale to assist the process of reproducibility between groups.

### **Acknowledgement**

The author thanks the management of VIT, Vellore, for the support and encouragement. The Chief Editor of Non-metallic materials Science Journal is also thanked for

the invitation to submit an article.

### **References**

- [1] Serope Kalpakjian, Steven R Schmid, *Manufacturing Processes for Engineering Materials*, 5th ed., Pearson Education India, 2009.
- [2] ASTM STM C-1684- 2018, *Standard Test Method for Flexural Strength of Advanced Ceramics at Ambient Temperature- Cylindrical Rod Strength*, West Conshohocken, PA, USA, 2018.
- [3] Richard L Lehman, Said K El-Rahaiby, John B Wachtman Jr., *Handbook on Fiber Ceramic Composites*, Purdue University, West Lafayette, IN, 1995.
- [4] [www.metallographic.com](http://www.metallographic.com)
- [5] YVRK Prasad, *Processing Maps: A Status Report*, *Jl. Of Materials Engineering and Performance*, December 2003, 12(6): 638-645.
- [6] George D Quinn, Brian T Sparenberg, Lewis K Ives, Said Jahanmir, Philip Koshy and Dwayne D Arola, *Flexural strength of ceramic and glass rods*, *Journal of Testing and Evaluation*, 2009, 37(3): 222-244. Paper ID JTE101649.

# Author Guidelines

This document provides some guidelines to authors for submission in order to work towards a seamless submission process. While complete adherence to the following guidelines is not enforced, authors should note that following through with the guidelines will be helpful in expediting the copyediting and proofreading processes, and allow for improved readability during the review process.

## I . Format

- Program: Microsoft Word (preferred)
- Font: Times New Roman
- Size: 12
- Style: Normal
- Paragraph: Justified
- Required Documents

## II . Cover Letter

All articles should include a cover letter as a separate document.

The cover letter should include:

- Names and affiliation of author(s)

The corresponding author should be identified.

Eg. Department, University, Province/City/State, Postal Code, Country

- A brief description of the novelty and importance of the findings detailed in the paper

Declaration

v Conflict of Interest

Examples of conflicts of interest include (but are not limited to):

- Research grants
- Honoria
- Employment or consultation
- Project sponsors
- Author's position on advisory boards or board of directors/management relationships
- Multiple affiliation
- Other financial relationships/support
- Informed Consent

This section confirms that written consent was obtained from all participants prior to the study.

- Ethical Approval

Eg. The paper received the ethical approval of XXX Ethics Committee.

- Trial Registration

Eg. Name of Trial Registry: Trial Registration Number

- Contributorship

The role(s) that each author undertook should be reflected in this section. This section affirms that each credited author has had a significant contribution to the article.

1. Main Manuscript

2. Reference List

3. Supplementary Data/Information

Supplementary figures, small tables, text etc.

As supplementary data/information is not copyedited/proofread, kindly ensure that the section is free from errors, and is presented clearly.

### **III. Abstract**

A general introduction to the research topic of the paper should be provided, along with a brief summary of its main results and implications. Kindly ensure the abstract is self-contained and remains readable to a wider audience. The abstract should also be kept to a maximum of 200 words.

Authors should also include 5-8 keywords after the abstract, separated by a semi-colon, avoiding the words already used in the title of the article.

Abstract and keywords should be reflected as font size 14.

### **IV. Title**

The title should not exceed 50 words. Authors are encouraged to keep their titles succinct and relevant.

Titles should be reflected as font size 26, and in bold type.

### **IV. Section Headings**

Section headings, sub-headings, and sub-subheadings should be differentiated by font size.

Section Headings: Font size 22, bold type

Sub-Headings: Font size 16, bold type

Sub-Subheadings: Font size 14, bold type

Main Manuscript Outline

### **V. Introduction**

The introduction should highlight the significance of the research conducted, in particular, in relation to current state of research in the field. A clear research objective should be conveyed within a single sentence.

### **VI. Methodology/Methods**

In this section, the methods used to obtain the results in the paper should be clearly elucidated. This allows readers to be able to replicate the study in the future. Authors should ensure that any references made to other research or experiments should be clearly cited.

### **VII. Results**

In this section, the results of experiments conducted should be detailed. The results should not be discussed at length in

this section. Alternatively, Results and Discussion can also be combined to a single section.

## **VIII. Discussion**

In this section, the results of the experiments conducted can be discussed in detail. Authors should discuss the direct and indirect implications of their findings, and also discuss if the results obtain reflect the current state of research in the field. Applications for the research should be discussed in this section. Suggestions for future research can also be discussed in this section.

## **IX. Conclusion**

This section offers closure for the paper. An effective conclusion will need to sum up the principal findings of the papers, and its implications for further research.

## **X. References**

References should be included as a separate page from the main manuscript. For parts of the manuscript that have referenced a particular source, a superscript (ie. [x]) should be included next to the referenced text.

[x] refers to the allocated number of the source under the Reference List (eg. [1], [2], [3])

In the References section, the corresponding source should be referenced as:

[x] Author(s). Article Title [Publication Type]. Journal Name, Vol. No., Issue No.: Page numbers. (DOI number)

## **XI. Glossary of Publication Type**

J = Journal/Magazine

M = Monograph/Book

C = (Article) Collection

D = Dissertation/Thesis

P = Patent

S = Standards

N = Newspapers

R = Reports

Kindly note that the order of appearance of the referenced source should follow its order of appearance in the main manuscript.

Graphs, Figures, Tables, and Equations

Graphs, figures and tables should be labelled closely below it and aligned to the center. Each data presentation type should be labelled as Graph, Figure, or Table, and its sequence should be in running order, separate from each other.

Equations should be aligned to the left, and numbered with in running order with its number in parenthesis (aligned right).

## **XII. Others**

Conflicts of interest, acknowledgements, and publication ethics should also be declared in the final version of the manuscript. Instructions have been provided as its counterpart under Cover Letter.

## About the Publisher

Bilingual Publishing Co. (BPC) is an international publisher of online, open access and scholarly peer-reviewed journals covering a wide range of academic disciplines including science, technology, medicine, engineering, education and social science. Reflecting the latest research from a broad sweep of subjects, our content is accessible world-wide—both in print and online.

BPC aims to provide an analytics as well as platform for information exchange and discussion that help organizations and professionals in advancing society for the betterment of mankind. BPC hopes to be indexed by well-known databases in order to expand its reach to the science community, and eventually grow to be a reputable publisher recognized by scholars and researchers around the world.

BPC adopts the Open Journal Systems, see on [ojs.bilpublishing.com](http://ojs.bilpublishing.com)

## Database Inclusion



Asia & Pacific Science  
Citation Index



Creative Commons



China National Knowledge  
Infrastructure



Google Scholar



Crossref



MyScienceWork

Bilingual Publishing Co. is a company registered in Singapore in 1984, whose office is at 12 Eu Tong Sen Street, #08-169, Singapore 059819, enjoying a high reputation in Southeast Asian countries, even around the world.



**BILINGUAL  
PUBLISHING CO.**  
Pioneer of Global Academics Since 1984

Tel: +65 65881289

E-mail: [contact@bipublishing.com](mailto:contact@bipublishing.com)

Website: [www.bipublishing.com](http://www.bipublishing.com)

ISSN 2661-3301



9 772661 330192